Superprotonic phase transition of $CsHSO_4$: A molecular dynamics simulation study

Calum R. I. Chisholm,[1] Yun Hee Jang,[2] Sossina M. Haile,[1] and William A. Goddard III[2,*]
[1]*Department of Materials Science, California Institute of Technology, Pasadena, California 91125, USA*
[2]*Materials and Process Simulation Center, Beckman Institute (139-74), California Institute of Technology, Pasadena, California 91125, USA*

(Received 14 July 2004; revised manuscript received 21 January 2005; published 7 October 2005)

The superprotonic phase transition (phase II → phase I; 414 K) of cesium hydrogen sulfate, $CsHSO_4$, was simulated using molecular dynamics with the "first principles" MSXX force field (FF). The structure, binding energy, and vibrational frequencies of the $CsHSO_4$ monomer, the binding energy of the $(H_2SO_4)_2$ dimer, and the torsion barrier of the HSO_4^- ion were determined from quantum mechanical calculations, and the parameters of the Dreiding FF for Cs, S, O, and H adjusted to reproduce these quantities. Each hydrogen atom was treated as bonded exclusively to a single oxygen atom (proton donor), but allowed to form hydrogen bonds to various second nearest oxygen atoms (proton acceptors). Fixed temperature-pressure (NPT) dynamics were employed to study the structure as a function of temperature from 298 to 723 K. In addition, the influence of several force field parameters, including the hydrogen torsional barrier height, hydrogen bond strength, and oxygen charge distribution, on the structural behavior of $CsHSO_4$ was probed. Although the FF does not allow proton migration (i.e., proton jumps) between oxygen atoms, a clear phase transition occurred as demonstrated by a discrete change of unit cell symmetry (monoclinic to tetragonal), cell volume, and molar enthalpy. The dynamics of the HSO_4^- group reorientational motion also changed dramatically at the transition. The observation of a transition to the expected tetragonal phase using a FF in which protons cannot migrate indicates that proton diffusion does not drive the transition to the superprotonic phase. Rather, high conductivity is a consequence of the rapid reorientations that occur in the high temperature phase. Furthermore, because no input from the superprotonic phase was employed in these simulations, it may be possible to employ MD to hypothesize superprotonic materials.

DOI: 10.1103/PhysRevB.72.134103 PACS number(s): 64.60.Cn, 66.10.Ed, 64.70.Kb

I. INTRODUCTION

Cesium hydrogen sulfate ($CsHSO_4$) and the analogs $MHXO_4$ (M=Rb,Cs;X=S,Se) (Ref. 1) belong to a class of compounds that exhibit "superprotonic" phase transitions resulting in fast protonic conduction at elevated temperatures. $CsHSO_4$ undergoes a phase transition from the low-temperature phase (phase II) to the high-temperature phase ("superprotonic" phase I) around 414 K.[2] Across this transition, the protonic conductivity increases by three to four orders of magnitude from $10^{-6}\ \Omega^{-1}\,cm^{-1}$ (phase II) to $10^{-3}-10^{-2}\ \Omega^{-1}\,cm^{-1}$ (phase I) (Ref. 3) as a result of structural changes that occur during the solid to solid, "superprotonic" phase transition. Proton conductors have applications in a wide variety of devices including electrochemical reactors, gas/humidity sensors, electrochromics (displays, windows, and mirrors), and, especially, fuel cells.[4] As solid state materials with very high conductivities,[5] the $MHXO_4$ compounds in their superprotonic phases are particularly attractive for these applications.

Although there have been molecular dynamics (MD) studies of the superprotonic phase of $CsHSO_4$,[6,7] focusing on the proton transfer and sulfate reorientation rates, there has not been an attempt to model the superprotonic phase transition of this compound. The present MD study was undertaken with two aims:

- To determine whether the superprotonic transition could be simulated without allowing proton migration and
- To predict the superprotonic phase transition in a well-known compound using a generalized procedure that can be applied to other solid acids for with little or no experimental data is available.

The first objective was motivated by the desire to ascertain whether proton hopping or tetrahedral reorientations are the essential ingredient in describing the transition from the ordered room temperature structure to the highly disordered superprotonic phase. The latter goal arises from the desire to greatly accelerate the discovery of new superprotonic compounds with improved properties for these applications. The utilization of classical MD methods, which ignore possible

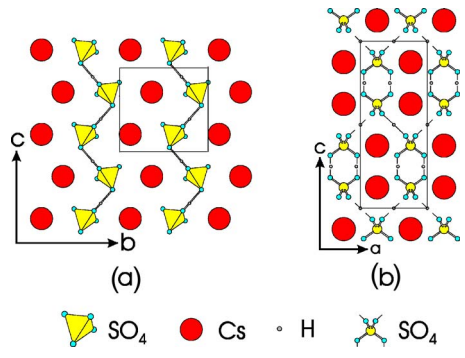

FIG. 1. (Color online) Crystal structure of $CsHSO_4$: (a) monoclinic phase II (Ref. 10) and (b) tetragonal phase I as proposed by Jirak *et al.* (Ref. 11). In (b), each oxygen position has half occupancy and the hydrogen atoms are placed in the middle of the disordered hydrogen bonds (dashed lines).

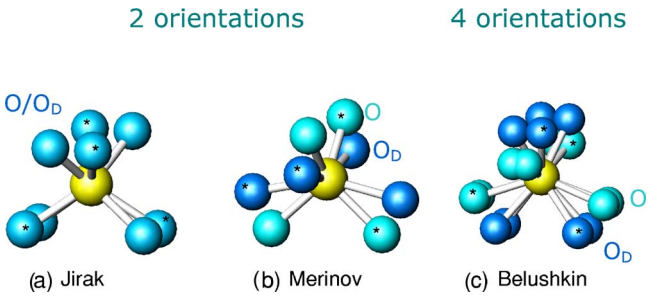

FIG. 2. (Color online) Possible configurations of the sulfate tetrahedra in the superprotonic phase: the structures by Jirak *et al.* (a), (Ref. 11), Merinov *et al.* (b), (Ref. 13), and Belushkin *et al.* (c), (Ref. 14) have two, two, and four orientations, respectively, which transform into each other by rotations of 32°, 30°, and 30°, respectively. The * designates one possible arrangement for the oxygen atoms of a tetrahedra.

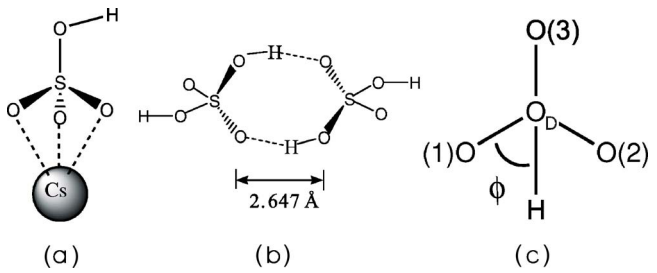

FIG. 3. (Color online) Structures used to adjust the FF parameters: (a) $CsHSO_4$ monomer, (b) $(H_2SO_4)_2$ dimer, and (c) HSO_4^- ion [projected down the S-O(H) bond]. The $CsHSO_4$ monomer (a) was used to determine the vdW parameters for Cs and all HSO_4^- FF parameters except for the hydrogen bond and the O-S-O-H torsional terms, which were adjusted with the results for (b) and (c), respectively.

quantum mechanical effects on the dynamics of the hydrogen bond, is justified in light of the high temperatures of the simulations.

Section II summarizes the important details of the low and high temperature phases of $CsHSO_4$ and elaborates on the nature of its superprotonic transition. Section III describes the *MSXX* force field (FF) used in these simulations and how it was developed from first principles. Section IV presents the results of the MD simulations using this FF. A summary and conclusions drawn from these MD simulations are given in Sec. V. The influence of selected FF parameters on the room and high temperature behavior of $CsHSO_4$ is presented in the Appendix.

II. PHYSICAL CHARACTERISTICS OF $CsHSO_4$

A. Polymorphs of $CsHSO_4$

There are three phases of crystalline $CsHSO_4$ that exist in the temperature range from room temperature to ~500 K under ambient pressures[8,9]

$$\text{phase III}(P2_1/c) \xrightarrow{330\text{–}370\ \text{K}} \text{phase II}(P2_1/c) \xrightarrow{410\text{–}415\ \text{K}} \text{phase I}(I4_1/\text{amd}).$$

Although phase III is the thermodynamically stable phase at room temperature (and the phase typically obtained from room temperature synthesis experiments) the simulations performed here utilized phase II as the starting point in order to focus on the transition at ~414 K to the superprotonic phase, phase I, without need to first reproduce the III → II transition. In the phase II structure,[10] sulfate groups are linked by hydrogen bonds so as to form zigzag chains along [001], Fig. 1(a). The $O_D-H,\ldots,O_A$ bonds are fully ordered (where O_D is the donor and O_A the acceptor in the hydrogen bond), with $<(O-H\cdots O)=174(6)°$, $d(O-H)=0.94(4)$ Å, $d(H\cdots O)=1.70(4)$ Å, and $d(O\cdots O)=2.636(5)$ Å.

The high temperature phase (phase I) is tetragonal (space group $I4_1/amd$), Fig. 1(b).[11] There is considerable disorder in the orientation of the hydrogen sulfate (HSO_4) groups (HSO_4 libration) in this phase,[12] with some debate as to the actual number and/or directions of the orientations possible for each tetrahedron, Fig. 2. According to Jirak *et al.*, who performed a powder neutron diffraction study on $CsHSO_4$ at a temperature slightly above 414 K, each tetrahedron adopts one of two orientations and the phase has lattice constants of $a=5.718(3)$ Å and $c=14.232(9)$ Å.[11] The structure put forward by Merinov *et al.*, based on a single crystal x-ray diffraction study of $CsDSO_4$ at 430 K, has lattice constants of $a=5.729(9)$ Å and $c=14.21(1)$ Å and four orientations for each tetrahedron.[13] A high-resolution neutron powder diffraction study by Belushkin *et al.* performed on $CsDSO_4$ at 448

TABLE I. Force field[a,b] for $CsHSO_4$.

$E=E^{\text{nonbond}}+E^{\text{valence}}$
$E^{\text{nonbond}}=E^{\text{Coulomb}}+E^{\text{vdW}}+E^{\text{H-bond}}$
$E^{\text{valence}}=E^{\text{bond}}_{\text{SO}}+E^{\text{angle}}_{\text{OSO}}+E^{RR}_{\text{OSO}}+E^{\theta\theta}_{\text{SOOO}}+E^{\text{bond}}_{\text{OH}}+E^{\text{angle}}_{\text{SOH}}+E^{\text{torsion}}_{\text{OSOH}}$
$E^{\text{Coulomb}}_{ij}(R)=C_0(q_iq_j/\varepsilon R_{ij})$
$E^{\text{vdW}}_{ij}(R)=D_0\{[(6/\zeta-6)e^{\zeta(1-R/R_0)}]-[(\zeta/\zeta-6)(R_0/R)^6]\}$
$E^{\text{H-bond}}_{\text{O-O}}(R)=D_0\{5(R_0/R)^{12}-6(R_0/R)^{10}\}$
$E^{\text{bond}}_{\text{SO}}(R)$ or $E^{\text{bond}}_{\text{OH}}(R)=1/2K_R(R-R_0)^2$
$E^{\text{angle}}_{\text{OSO}}(\theta)$ or $E^{\text{angle}}_{\text{SOH}}(\theta)=(1/2)K_\theta/\sin^2\theta_0(\cos\theta-\cos\theta_0)^2$
$E^{RR}_{\text{OSO}}(R_1,R_2)=K_{RR}(R_1-R_0)(R_2-R_0)$
$E^{\theta\theta}_{\text{SOOO}}(\theta_1,\theta_2)=\left(K_{\theta\theta}/\sin\theta_{0_1}\sin\theta_{0_2}\right)(\cos\theta_1-\cos\theta_{0_1})(\cos\theta_2-\cos\theta_{0_2})$
$E^{\text{torsion}}_{\text{OSOH}}(\varphi)=1/2K_\varphi[1+\cos(3\varphi)]$

[a]Nonbonding interaction are excluded for 1,2-pairs (bonded atoms) and 1,3-pairs (atoms bonded to a common atom).
[b]The constants in E^{Coulomb} are the dielectric constant ($\varepsilon=1$) and $C_0=332.0637$ (the unit conversion factor when atomic charges are in electron units ($|e|$), the distance R is in angstroms, and E_{Coulomb} is in kcal/mole).

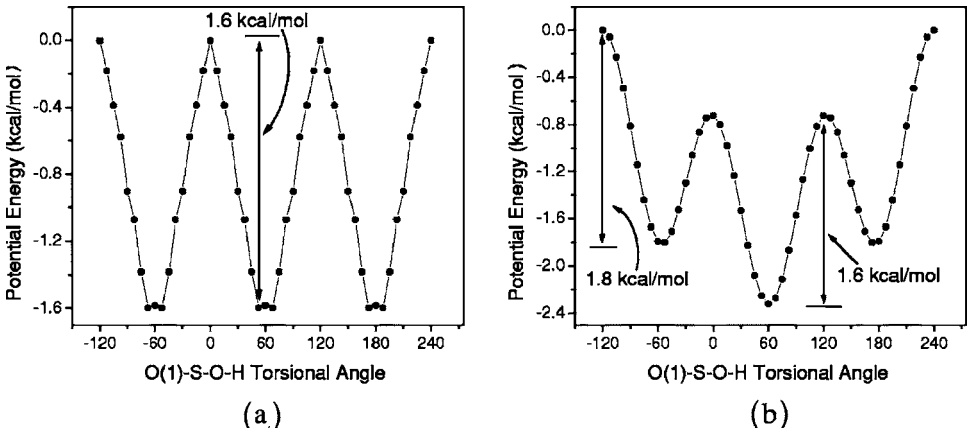

FIG. 4. Potential energy curves for a HSO_4^- ion with fixed O(1)-S-O_D-H torsional angles: (a) optimized by QM and (b) minimized with the adjusted FF. The calculations were carried out from 0° to 60° and extended over a full 360° using symmetry.

K, gave lattice parameters of $a=5.741\,47(9)$ Å and $c=14.315\,08(26)$ Å and also four orientations for each tetrahedron,[14] but with directions that differ from those proposed by Merinov *et al.*

B. Nature of the superprotonic transition of $CsHSO_4$

Regardless of which structure is selected for $CsHSO_4$ phase I, the basic nature of the phase transition and mechanism of proton conduction remain the same. The transition is

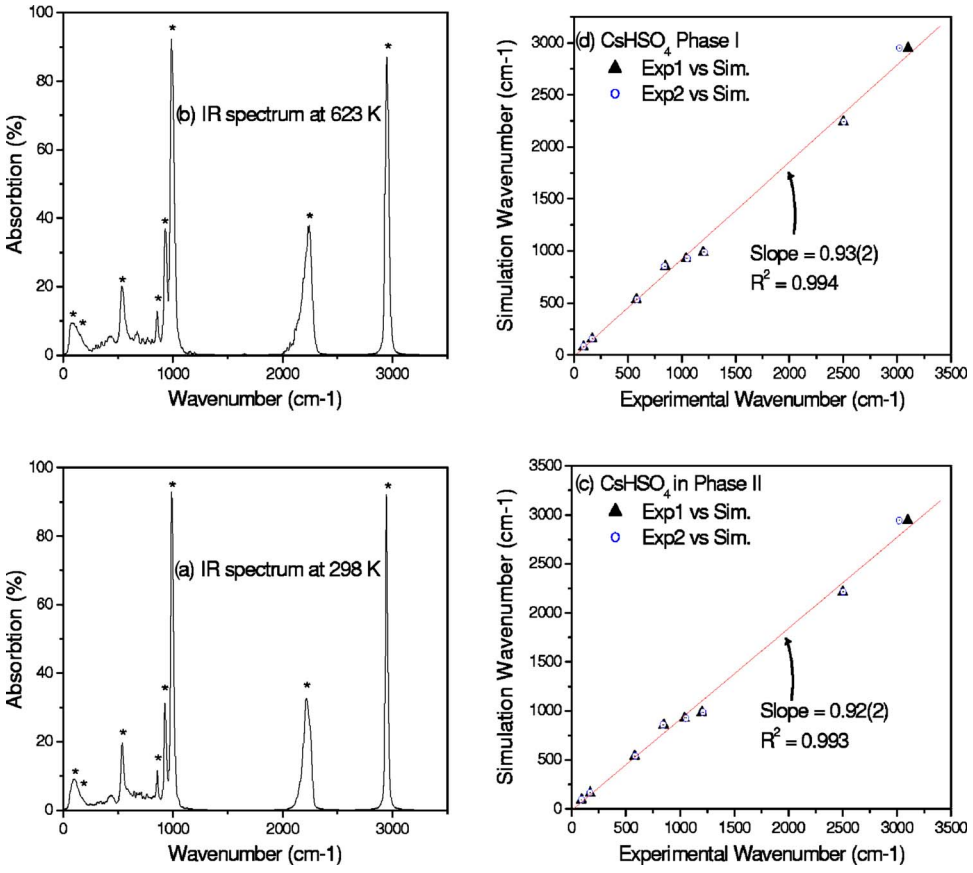

FIG. 5. (Color online) Calculated IR spectra for MD simulations: For phases II and I of $CsHSO_4$, (a) and (b), respectively. Peaks with strongest absorption are marked with an asterisk and the frequencies at the peak maximums are compared to those of the strongest peaks found by two separate infrared spectroscopy experiments on polycrystalline $CsHSO_4$ (Refs. 20 and 36). In both phase II (c) and phase I (d) the simulation and experimental peak positions are very similar (for perfect match ⇒ slope=1). A plot of the experimental values below versus those above the superprotonic transition (not shown) results in a slope of 0.98(1), $R^2=0.999$, as the measured IR spectra changes little over the phase II-I transition.

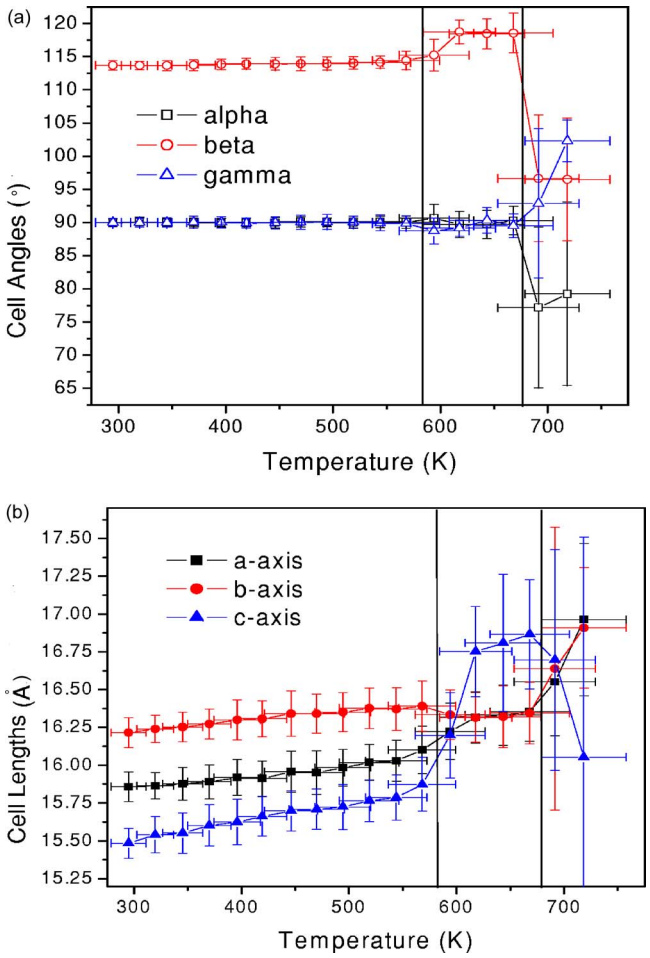

FIG. 6. (Color online) Cell parameters as a function of temperature (MD simulations): average values calculated from the final 150 ps of each 300 ps simulation. Lines indicate the two transitions at 598 and 698 K.

of first order from the ordered, low symmetry phase to the disordered high symmetry phase.[14] Below the transition, the HSO_4 group orientation is believed to be static, whereas above the transition, rapid reorientations of the tetrahedral unit occurs.[15] Since the protonic conductivity is a direct result of these tetrahedral reorientations, the high conductivity of phase I is a by-product of the ideal structure.[16]

H^+ NMR measurements and quasielastic neutron scattering (QNS) experiments on $CsHSO_4$ confirm a high rate of proton diffusion in the compound when it is in its superprotonic phase. Both methods found a proton diffusion constant D_H of $\sim 1 \times 10^{-7}$ cm^2/s at temperatures above 414 K.[17] RF-microwave dielectric measurements indicate that the sulfate tetrahedra undergo fast reorientations (10^{12} Hz) while proton transfer occurs more slowly (10^9 Hz).[15]

Based on such analyses the proton transfer process in phase I is thought to consist of two steps:

- Creation of hydrogen bonds between previously isolated tetrahedra by HSO_4^- rotations and
- Translation of protons between the two equilibrium sites in the newly created O-H···O bond resulting in H_2SO_4 and SO_4^- defects.[5]

The "doubly protonated" H_2SO_4 defect and the "deprotonated" SO_4 defect may then propagate by classical hopping of protons between the two minima in the O-H···O bonds along the H-bonded chains.[17] The IR spectra of phases II and I $CsHSO_4$ are almost identical, and thus the local geometry and modes of the SO_4 groups are unaffected by the transition and do not contribute to the enhanced conductivity.[18–20] However, the librations/reorientations of the HSO_4 groups in phase I allow the weak link H-acceptor hydrogen bonds to break, while the strong link H-donor bonds are preserved. On account of rapid rotation of the sulfate groups, the proton samples all possible crystallographic positions, with translation of the proton along a newly formed two-minimum hydrogen bond occurring once in about a hundred to a thousand reorientations of the tetrahedra. Thus, migration of protons is affected both by their jumping between positions on the hydrogen bond and by reorientations of HSO_4 groups. Such a process is an example of the Grotthuss mechanism of proton conduction.[1]

III. *MSXX* FORCE FIELD FOR $CsHSO_4$

Simulations of $CsHSO_4$ were carried out here using a Drieding-like force field (FF) (Ref. 21) in which selected parameters were adjusted from the Dreiding defaults to fit quantum mechanical (QM) calculations performed on small clusters involving the elements of $CsHSO_4$. The functional forms and parameters of the adjusted Drieding FF are given in Tables I and II, respectively. The types of interactions are separated into nonbonding (Coulombic, Van der Waals, and hydrogen bond) and valence (or bonding) interactions. Nonbonding interactions between bonded atoms (1,2 pairs) and between those bonded to a common atom (1,3 pairs) are excluded. The off-diagonal van der Waals (vdW) parameters (Cs-O, Cs-S, Cs-H, S-O, S-H, and O-H) were determined from the diagonal vdW parameters (Cs-Cs, S-S, O-O, and H-H) by the standard combination rule.[21]

In this force field, the chemical nature of each atom in the structure is defined at the outset, and that identity is retained, regardless of structural transitions. In particular, the donor in the hydrogen bond remains the donor under all conditions. Accordingly, the hydrogen is always bonded to a specific (donor) oxygen atom. The acceptor in the hydrogen bond is defined simply as the second nearest oxygen neighbor (regardless of its identity otherwise). In the initial structural state of phase II, the acceptor is well-defined and is assigned a slightly different charge than the remaining two oxygen atoms of the sulfate group. Proton diffusion (or transfer) from one oxygen atom to another is not permitted with this kind of force field. Thus, the FF cannot describe any structural properties of $CsHSO_4$ that result specifically from proton migration.[5] While this constraint might be viewed as describing an unrealistic situation, it allows one, in fact, to separate out the contributions of proton transfer from other phenomenon on the superprotonic phase transition.

The FF parameters were adjusted to reproduce three separate quantum mechanical (QM) calculations performed using the B3LYP flavor of density functional theory (DFT) and using the (LACVP**) basis and pseudopotential[24–29]

TABLE II. Force field parameters for $CsHSO_4$.[a]

E^{vdW}	Cs[l]	R_o[b]	4.1741[i]	D_o[c]	0.37[i]	ζ	18[i]
	S[l]	R_o[b]	4.03[h]	D_o[c]	0.344[h]	ζ	12.0[h]
	O[l]	R_o[b]	3.4046[h]	D_o[c]	0.0957[h]	ζ	13.483[h]
	H[l]	R_o[b]	3.195[h]	D_o[c]	0.0001[h]	ζ	12.0[h]
E^{bond}	$S\text{-}O_D$	R_o[b]	1.6925[i]	K_b[d]	700.0[h]		
	$S\text{-}O_A$	R_o[b]	1.499[i]	K_b[d]	700.0[h]		
	$O_H\text{-}H$	R_o[b]	0.988[i]	K_b[d]	700.0[h]		
E^{angle}	$O_A\text{-}S\text{-}O_D$	θ_o[e]	105.933[i]	K_θ[f]	350.0[h]		
	$O_A\text{-}S\text{-}O_A$	θ_o[e]	115.2[i]	K_θ[f]	350.0[h]		
	$S\text{-}O_D\text{-}H$	θ_o[e]	109[i]	K_θ[f]	350.0[h]		
E^{RR}	$O_A\text{-}S\text{-}O_A$	$R_o(O_A)$[b]	1.4856[i]	$R_o(O_A)$[b]	1.4856[i]	K_{RR}[d]	102.0[m]
E^{RR}	$O_A\text{-}S\text{-}O_D$	$R_o(O_A)$[b]	1.4856[i]	$R_o(O_D)$[b]	1.65[i]	K_{RR}[d]	102.0[m]
$E^{\theta\theta}$	$S\text{-}O_A\text{-}O_A\text{-}O_A$	$\theta_o(O_A,O_A)$[e]	112.8[i]	$K_{\theta\theta}$[f,g]	72.5[h]		
	$S\text{-}O_A\text{-}O_A\text{-}O_D$	$\theta_o(O_A,O_D)$[e]	105.933[i]	$K_{\theta\theta}$[f,g]	72.5[h]		
	$S\text{-}O_A\text{-}O_D\text{-}O_A$	$\theta_o(O_A,O_A)$[e]	112.8[i]	$\theta_o(O_A,O_D)$[e]	105.933[i]	$K_{\theta\theta}$[f,g]	72.5[h]
$E^{torsion}$	$O_A\text{-}S\text{-}O_D\text{-}H$	K_φ[c]	2.1669[j]				
E^{bond}	$O_D\cdots O_A$	R_o[b]	3.004[k]	D_o[c]	0.2366[k]		

[a]For functional forms, see Table I.
[b]In angstroms.
[c]In kcal/mol.
[d]In kcal/mol/Å (Ref. 2).
[e]In degrees.
[f]In kcal/mol/rad (Ref. 2).
[g]In the current version of POLYGRAF (version 3.30), the divisor for angle-angle cross term $E^{\theta\theta}$ is written as $E^{\theta\theta}(\cos\theta_1-\cos\theta_{10})(\cos\theta_2-\cos\theta_{20})$ where $E^{\theta\theta}=K_{\theta\theta}/\sin\theta_{0_1}\sin\theta_{0_2}=81.5625$ where $K_{\theta\theta}=72.5$. In Cerius (Ref. 2) the input is in terms of $K_{\theta\theta}$ (Ref. 22).
[h]From Dreiding FF (Ref. 21).
[i]Adjusted to reproduce a $CsHSO_4$ monomer's QM structure, binding energy, and frequencies.
[j]Adjusted to reproduce QM torsion barrier height (in kcal/mol) for HSO_4^- ion in a dielectric medium with a relative dielectric constant of 10.
[k]Adjusted to fit the QM O-O distance and binding energy of a $H_2SO_4-H_2SO_4$ dimer.
[l]The off-diagonal van der Waals (vdW) parameters (Cs-O, Cs-S, Cs-H, S-O, S-H, and O-H) are determined from the diagonal vdW parameters (Cs-Cs, S-S, O-O, and H-H) by the standard combination rule (Ref. 21).
[m]From previous work on MSO_4 (M=Ba, Sr, Ca) (Ref. 23).

(LACVP** denotes that all electrons are described on H/O/S using the 6-31G** basis set while the Xe core of Cs is described with the LACVP effective core potential and basis set). All quantum mechanical calculations were carried out using the JAGUAR QM software suite.[30]

These calculations were carried out for the gas-phase $CsHSO_4$ monomer, the gas-phase $(H_2SO_4)_2$ dimer, and a HSO_4^- ion in a Poisson-Boltzmann continuum solvent[31] with a dielectric constant of 10 and a solvent radius of 2.39 Å (Fig. 3). The FF parameters were adjusted so that each chemical species would duplicate the results of the QM calculations after a FF minimization to lowest potential energy. All FF energy minimizations were carried out with the Newton-Raphson method using the CERIUS2 software.[22] Further detail is given below.

A. $CsHSO_4$ gas phase monomer

1. Charges

The HSO_4^- group of the $CsHSO_4$ gas-phase monomer, which, in principle, has one donor oxygen atom and three, non hydrogen-bonded oxygen atoms, Fig. 3(a), is taken to be a reasonable approximation of the bisulfate group in the $CsHSO_4$ crystal. In the crystal and below the transition, this group has one donor oxygen atom, one acceptor, and two oxygen atoms that do not participate in hydrogen bond formation. Above the transition, the four oxygen atoms become chemically equivalent. The electrostatic-potential-fitted (ESP) charges of the four oxygen atoms of the gas-phase $CsHSO_4$ monomer, calculated from the QM wave function,[32] differed significantly from one another, Table III. As might

TABLE III. ESP charges for $CsHSO_4$: From the QM calculation on the $CsHSO_4$ monomer [B3LYP/LACVP**] and the final set used in the simulations.

Environment	$q_{Cs}(\lvert e\rvert)$	$q_S(\lvert e\rvert)$	$q_{O(1)}(\lvert e\rvert)$	$q_{O(2)}(\lvert e\rvert)$	$q_{O(3)}(\lvert e\rvert)$	$q_{OD}(\lvert e\rvert)$	$q_H(\lvert e\rvert)$
Gas-phase	0.928	1.045	−0.630	−0.636	−0.588	−0.523	0.404
Simulation	1.0	1.045	−0.651	−0.651	−0.606	−0.541	0.404

TABLE IV. Phase II at 298 K: Simulation versus experiment.

Parameter	MD at 298 K	Experiment-x ray[a]	Experiment-neutron[b]	Error vs x ray
Density (g/cm^3)	3.35(3)	3.338(3)	3.3429(1)	0.36%
a (Å)	7.93(5)	7.781(2)	7.78013(9)	1.91%
b (Å)	8.11(5)	8.147(2)	8.13916(2)	0.45%
c (Å)	7.74(5)	7.722(2)	7.72187(9)	0.26%
α (°)	90.0(6)	90	90	0%
β (°)	113.7(7)	110.775(13)	110.8720(4)	2.6%
γ (°)	90.0(6)	90	90	0%

[a]From single-crystal x-ray diffraction on $CsHSO_4$ at 298 K (Ref. 10).
[b]From the high-resolution neutron powder diffraction study of $CsDSO_4$ at 300 K (Ref. 14).

be expected, the magnitude of the charge was smallest on the donor oxygen atom. Of the remaining three atoms, two, O(1) and O(2) had comparable (and larger) charges whereas O(3) had an intermediate value of charge. Accordingly, the O(3) atom fulfills the role of the acceptor oxygen, without explicitly introducing hydrogen bonds.

For the simulations, the charges of the Cs and O atoms obtained from the QM calculations were slightly modified, whereas those of the S and H atoms were utilized directly. Specifically, the QM charge on Cs of $+0.928|e|$ was increased to $+1.0|e|$ in order to accommodate changes about the Cs environment during the simulation. This increase in charge was balanced by an increase in the magnitude of the charge on each of the oxygen atoms by $0.018|e|$. The adjusted charges of the O(1) and O(2) oxygen atoms (now, $-0.648|e|$ and $-0.654|e|$, respectively) were then averaged (giving a final charge of $-0.651|e|$ each) to reflect the chemical similarity between these atoms in the crystalline structure.

2. Nonelectrostatic parameters

Given the charges, the vdW parameters for Cs and the FF parameters for HSO_4^- were adjusted to reproduce the QM calculation on the gas-phase $CsHSO_4$ monomer. This optimized structure has the Cs atom near the threefold axis of symmetry of the tetrahedral face opposite the hydrogen bonded oxygen, Fig. 3(a). The vdW parameters for cesium were determined to reproduce three terms: the average Cs-O distance for the three non-hydrogen bonded oxygens, the binding energy of the Cs^+ to the HSO_4^- ion, and the symmetric stretch frequency describing the Cs vibration with the HSO_4 monomer (the Cs-HSO_4 stretching mode).

Except for torsional and hydrogen bond parameters, the valence FF parameters for S, O, and H in HSO_4^-, were adjusted to fit the QM structure (bond lengths and angles) and frequencies of the HSO_4^- ion. This is a straightforward process, except for the complexity of defining force field parameters for the donor oxygen atom that were distinct from those of the other oxygen atoms. Such a distinction is a direct result of having fixed the protons to particular oxygen atoms. Nevertheless, the final FF distances, angles, and frequencies were all within 1% of their respective QM values.

3. Classification of oxygen atoms

There are then essentially three types of oxygen atoms in this force field:

- Donor atoms: O_D, have a distinct set of FF parameters (O_D values) and charge ($-0.541|e|$).
- Acceptor atoms. O(3), have O_A FF parameters and a charge of $-0.606|e|$.
- Non hydrogen-bonded atoms: O(1) and O(2), have O_A FF parameters and a charge of $-0.651|e|$.

This classification of the oxygen atoms results from the inequivalence of the S-O bonds in the HSO_4^- ion. Because the O_D atom forms a bond to hydrogen, the bond between it and sulfur, S-O_D, is a single bond, whereas the S-O(1),O(2),O(3) bonds have an average bond order of 5/3. The O(3) atom is taken to be the acceptor oxygen in the hydrogen bond because the QM calculation shows this atom to have a smaller charge than the O(1) and O(2) atoms. The acceptor oxygen atom would be expected to have a charge intermediate between that of the donor oxygen atom and of the two non hydrogen-bonded oxygen atoms.

B. $(H_2SO_4)_2$ gas phase dimer

Quantum mechanical calculations on the gas-phase $(H_2SO_4)_2$ dimer were used to establish the FF parameters of the hydrogen bond. While keeping the FF parameters for S, O, and H fixed at the optimized values determined above , see Table II, the hydrogen bond parameters (R_o and D_o) were varied to reproduce the QM calculated O-O distance (2.647 Å) and binding energy (-18.569 kcal/mole) of the $(H_2SO_4)_2$ dimer. The atomic charges where set to the as-calculated values obtained from the QM calculation, Table III (line 2), because the calculated FF binding energy was observed to be highly dependent on the charges of the atoms. Hence, unrealistic hydrogen bond parameters were required to match the FF calculated binding energy to the QM value using the adjusted atomic charges described in Sec. III A 1. Because each H_2SO_4 group has two donor oxygen atoms (as opposed to just one for the $CsHSO_4$ monomer from which the FF parameters were obtained), the H_2SO_4 tetrahedra were somewhat distorted from the QM structure upon minimization of the dimer energy using the FF parameters of Table II. These slight distortions (in bond lengths and angles) were ignored

TABLE V. Average atomic positions from the MD simulation at 298 K.

Atom	MD at 298 K			Experiment at 293 K[a]			Deviation
	x/a	y/b	z/c	x/a	y/b	z/c	$\left(\frac{\Delta x^2+\Delta y^2+\Delta z^2}{3}\right)^{1/2}$
Cs	0.22(2)	0.12(2)	0.22(2)	0.21551(4)	0.12907(3)	0.20605(4)	0.009
S	0.75(2)	0.11(2)	0.27(2)	0.75214(14)	0.12727(12)	0.27996(14)	0.012
O_D	0.60(3)	0.20(3)	0.09(3)	0.5890(5)	0.2207(5)	0.1312(6)	0.025
$O_A(2)$	0.65(3)	0.03(4)	0.37(3)	0.6647(5)	0.0700(4)	0.4079(5)	0.035
O(3)	0.87(4)	0.24(2)	0.88(3)	0.8947(5)	0.2536(4)	0.8594(5)	0.021
O(4)	0.83(4)	1.00(4)	0.20(4)	0.8062(6)	0.9960(4)	0.1867(5)	0.017
H	0.66(4)	0.25(3)	0.02(2)	0.625(8)	0.295(6)	0.057(7)	0.040

[a]From single crystal x-ray diffraction on $CsHSO_4$ at 298 K (Ref. 10).

during the process of adjusting the hydrogen bond R_o and D_o values to match the FF minimized O-O distance and binding energy of the $(H_2SO_4)_2$ dimer to the QM values.

C. HSO_4^- ion in dielectric medium

At this stage only one FF parameter remained to be determined: the energy barrier for torsion of the O-S-O-H angle (K_φ in Tables I and II). To obtain this parameter, QM calculations were carried out on an isolated HSO_4^- ion placed in a Poisson-Boltzmann continuum solvent (PBF) of dielectric constant of 10. This approximates the experimental value of the dielectric constant of $CsHSO_4$ (phase II), also ~10, determined by impedance spectroscopy.[2] The PBF formalism[31] uses a realistic, solvent-accessible surface based on a solvent radius of 2.39 Å plus the dielectric constant to describe the polarization of the solvent due to the electrostatic field of the solute. The forces on the solute due to the reaction surface are then calculated to obtain the optimum structure in the solvent. The torsion angle, O(1)-S-O_D-H, of the HSO_4 ion was varied from 60° to 0° in steps of 7.5°, and QM calculations were carried out for each configuration. The structure was relaxed for each (fixed) value of the torsion angle and the energy of the structure computed, Fig. 4. The QM barrier [the potential energy difference between the minimum (~52.5°) and maximum (at 0°)] for torsion of the O(1)-S-O_D-H bond was found to be 1.6 kcal/mol.

To obtain a FF parameter K_φ that similarly yielded a barrier height of 1.6 kcal/mol, analogous calculations for each of the values of the torsion angle were carried out in the FF formalism. However, in each QM optimized structure, the oxygen atoms nearest the hydrogen had charges similar to O(1) and O(2) in Table III, while the oxygen farthest from the hydrogen had a charge similar to O(3). Hence, this procedure leads to an asymmetry in the FF barrier height due to the differences in the fixed oxygen charges used, Fig. 4(b), but nevertheless does yield a FF that properly reproduces the torsion barrier height.

IV. RESULTS OF MD SIMULATIONS

The structure of phase II of $CsHSO_4$ was optimized using the Newton-Raphson method with periodic boundary conditions. The simulation unit consisted of a $2\times2\times2$ supercell including 32 $CsHSO_4$ units. A series of MD simulations (NPT) were carried out at various temperatures from 298 to 723 K in 25 K steps using a Nosé-Hoover thermostat to maintain the temperature and a Rahman-Parrinello barostat to maintain the pressure at 1 atm.[33,34] For each temperature the MD calculation was carried out for 300 ps with a time step of 1 fs. Properties (potential energy, lattice constants, HSO_4^- orientation, etc.) were calculated from the average over the final 150 ps, unless stated otherwise. All the simulations were carried out using the CERIUS2 software package.[22]

A. Phase II at room temperature: Simulation versus experiment

Table IV shows that the average structural parameters (density and cell parameters) obtained from the MD simula-

TABLE VI. Comparison between MD[a] and experiment for the structural parameters of hydrogen bonds in phase II.

	Optimized $(H_2SO_4)_2$ dimer	MD at 298 K	Experiment-x ray[b]	Experiment-neutron[c]	Error (%) versus x-ray
$r(O_D\text{-}H)$ (Å)	1.001	0.99±0.07	0.94±0.04	0.983±0.005	5
$r(H\cdots O_A)$ (Å)	1.651	2.03±0.4	1.70±0.04	1.667±0.008	28
$r(O_D\cdots O_A)$ (Å)	2.647	2.77±0.16	2.636±0.005	2.633±0.005	11
$<(O_DHO_A)$ (°)	173.4	130±24	174±6	166.6±0.6	25

[a]Values calculated by totaling the distance/angle for each snap shot from 150–300 ps and then averaging over the 1500 snap shots.
[b]From single crystal x-ray diffraction on $CsHSO_4$ at 298 K (Ref. 10).
[c]From the high-resolution neutron powder diffraction study of $CsDSO_4$ at 300 K (Ref. 14).

TABLE VII. HSO_4 group arrangement: QM and FF calcution versus MD and experimental values.

	Optimized $CsHSO_4$ monomer	FF Min. $CsHSO_4$ monomer	MD: phase II (at 298 K)	Experiment x ray[a] (at 298 K)	Experiment neutron[b] (at 300 K)
r(S-O)(Å)	1.488, 1.487	1.484, 1.484	1.48(3), 1.48(3)	1.438(3), 1.433(3)	1.430(5), 1.435(9)
$r(S\text{-}O_D)$(Å)	1.650	1.650	1.65(3)	1.573(4)	1.589(8)
$r(S\text{-}O_A)$(Å)	1.479	1.487	1.49(3)	1.461(3)	1.472(5)
$<(SO_DH)$(°)	105.9	105.9	106(3)	114.7(4)	110.6(6)
$<(OSO_D)$(°)	107.3, 106.6, 103.9	107.0, 105.3, 105.3	105(2), 104(2), 104(2)	107.4(2), 106.6(2), 101.5(2)	107.5(5), 106.9(4), 101.9(5)
<(OSO)(°)	113.5, 113.1, 111.8	113.0, 113.0, 112.3	114(2), 114(2), 114(2)	113.6(2), 113.5(2), 113.1(2)	114.2(6), 113.4(5), 111.9(5)
<OSOH	53.1	60.6	60(15)	42.2(4), 79.7(3)	47.3(7), 75.6(7)
$r(\overline{Cs\text{-}O_{nn}})$(Å)	3.218	3.217	3.16(27)	3.220(4)	3.218(6)

[a]From single crystal x-ray diffraction on $CsHSO_4$ at 298 K (Ref. 10).
[b]From the high-resolution neutron powder diffraction study of $CsDSO_4$ at 300 K (Ref. 14).

tion at 298 K are within a few percent of the experimental values. Similarly, Table V shows that the atomic coordinates are almost all within experimental uncertainties of the published values. The largest differences between the experimental and calculated atomic positions (i.e., the deviations) occur for the atoms which participate in the hydrogen bonds (O_D, O_A, and H), Tables V and VI. These differences likely arise from the large thermal fluctuations of the hydrogen atoms,[35] as well as the observed threefold rotations of the sulfate groups around the S-O_D bonds described below. The bond lengths and angles of the HSO_4 groups from the simulation are compared to the experimental values in Table VII. The calculated S-O, S-OA, and S-O_D bond lengths are each somewhat too long, by amounts of 0.05, 0.02, and 0.06 Å, respectively. The SO_DH bond angle of 106° is 4.6° smaller than experiment, whereas the average OSO_D is only 1° smaller and the OSO angles from MD and experiment agree exceptionally well, both ~114°. Turning to the Cs coordination sphere, we note that the mean Cs-O distance is too short by 0.06 Å.

TABLE VIII. MD versus experimental parameter for the terragonal phase I $CaHSO_4$.

Parameter	MD (at 623 K)	Experiment-neutron[a] (at 414 K)	Experiment-x ray[b] (at 430 K)	Experiment-neutron[c] (at 448 K)
Density (g/cm^3)	3.13(5)	3.282(6)	3.27(2)	3.2366(2)
a (Å)	5.77(17)	5.718(3)	5.729(9)	5.74147(9)
b (Å)	5.77(17)	5.718(3)	5.729(9)	5.74147(9)
c (Å)	14.66(54)	14.232(9)	14.21(1)	14.31508(26)
α (°)	90(2)	90	90	90
β (°)	90(2)	90	90	90
γ (°)	90(1)	90	90	90
r(S-O)(Å)	1.65(4), 1.49(4), 1.48(4), 1.48(4)	4×1.48(2)	2×1.46(5), 2×1.48(7)	2×1.504(10), 2×1.570(5)
<(OSO)(°)	114(4), 114(4), 114(4), 114(3), 104(3), 104(3)	2×111.9(8), 4×108.3(9)	125.5(9),95.5(8), 2×116.8(8), 2×98.2(10)	112.5(3),112.5(3) 108.9(3),108.9(2) 107.2(2), 107.1(4)
$r(O_D-O_A)$(Å)	2.9(3)	8×2.79(4)	4×2.84(6)	16×2.59(1), 8×2.806(18)
$r(\overline{Cs-O_{nn}})$(Å)(Å)	3.17(34)	3.17(2)	3.18(4)	3.248(7)

[a]From the neutron powder diffraction study of $CsHSO_4$ at 414 K (Ref. 11).
[b]From the neutron powder diffraction study of $CsDSO_4$ at 430 K (Ref. 13)
[c]From the high-resolution neutron powder diffraction study of $CsDSO_4$ at 448 K (Ref. 14).

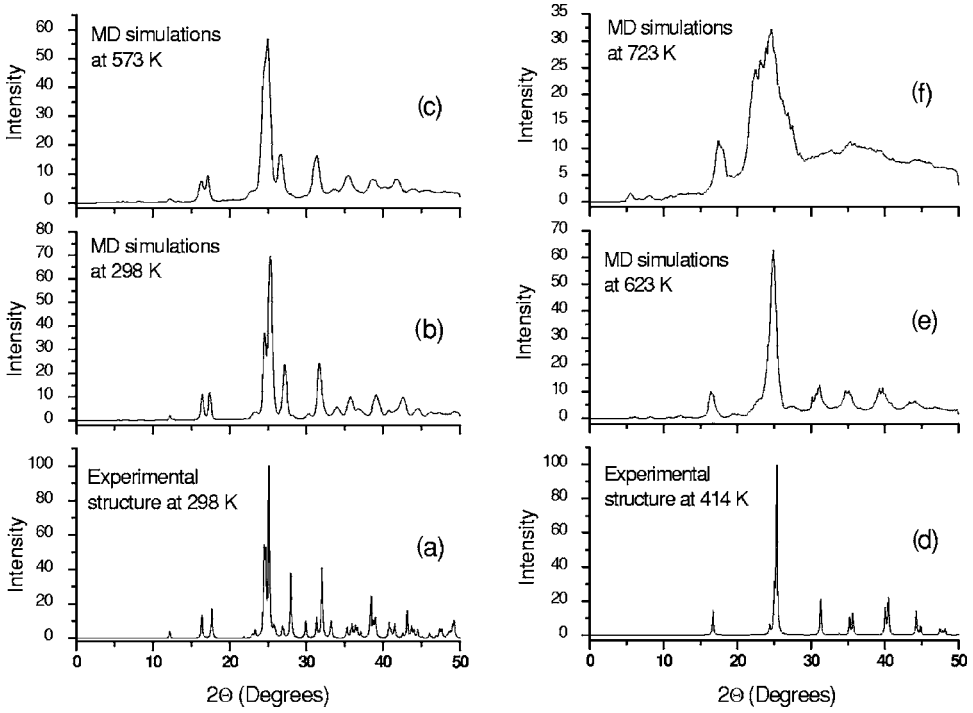

FIG. 7. Calculated x-ray powder diffraction patterns (time averaged from 150 ps of MD, 1500 frames). (a) Phase II $CsHSO_4$ calculated from the experimental structure (Ref. 10). (b) and (c) Phase II calculated from MD simulations at 298 and 573 K, respectively. (d) Phase I $CsHSO_4$ calculated from the Jirak *et al.* experimental structure (Ref. 11). (e) Phase I calculated from MD simulations at 623 K. (d) X-ray diffraction pattern calculated from MD simulations at 723 K, above the second (melting) transition.

Additional evaluation of the FF model can be gained by comparison of the experimental and simulated IR spectra. The simulated spectrum was generated by taking the average of 30 spectra, calculated every 5 ps from 150 to 300 ps (using CERIUS2[22]). The comparison is provided in Fig. 5. The positions of the adsorption bands from experiment and simulation match exceptionally well, and, again, validate the computational approach developed here.

In sum, the *MSXX* FF developed here reproduces the structure of phase II $CsHSO_4$ well at both the global (unit cell) and local (interatomic bonding) scales, despite the fact that no structure specific information from phase II was input into the FF model. Furthermore, the structural values obtained from the MD simulations faithfully reproduce those obtained from the quantum mechanical calculations on clusters. Thus, the small differences between experimental and simulated values are likely due to solid state effects that are not accounted for in the QM calculations, including such things as hydrogen migration and molecular polarizability. It would be straightforward to modify the FF parameters to agree much more closely to the experimental phase II structure. We chose not to do so because a major goal of this work is to develop an approach that can be used in the absence of experimental data. The present study of $CsHSO_4$, for which there is ample experimental data, serves as a testbed to calibrate how well this first principles or molecular based approach can predict the bulk phase transition behavior of superprotonic conductors.

B. Phase transition: Static properties

1. Cell parameters and local structural features

The average cell parameters, a, b, c, α, β, and γ are plotted as a function of temperature in Fig. 6. At 598 K, these parameters undergo a dramatic change, suggesting a phase transition. In particular, the b and c lattice parameters become equal in magnitude and the angle β becomes $\sim 120°$. These are exactly the changes expected for the monoclinic to tetragonal transition. The cell vectors of the monoclinic phase ($\vec{a}_m, \vec{b}_m$, and $\vec{c}_m$) are related to those of the tetragonal phase ($\vec{a}_t, \vec{b}_t$, and $\vec{c}_t$) as follows:[13]

TABLE IX. MD versus experimental parameters for the tetragonal phase I $CsHSO_4$.

	MD at 623 K			Experiments above 414 K[a]			Deviation
	x/a	y/b	z/c	x/a	y/b	z/c	$[(\Delta x^2+\Delta y^2+\Delta z^2)/3]^{1/2}$
Cs	0.501(16)	0.249(9)	0.124(17)	0.5	0.25	0.125	0.0010
S	0.002(11)	0.749(7)	0.125(6)	0	0.75	0.125	0.0015

[a]From x-ray and neutron diffraction studies of $CsHSO_4$ above 414 K (Refs. 11, 13, and 14).

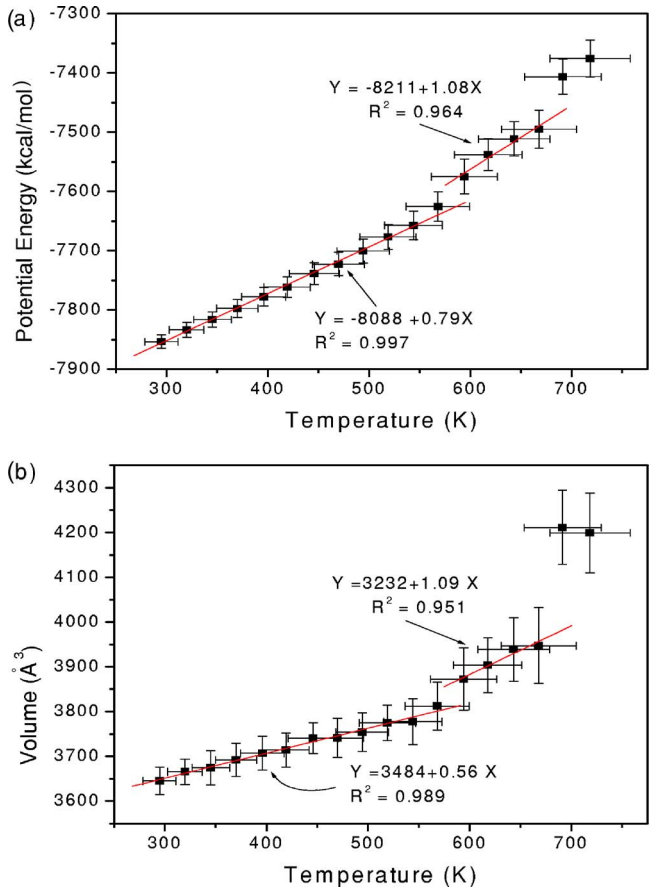

FIG. 8. (Color online) (a) Potential energy and (b) volume as a function of temperature from MD simulations: 298 k to 723 k.

$$\vec{a}_t = \frac{1}{2}(\vec{a}_m + \vec{b}_m), \quad \vec{b}_t = \frac{1}{2}(\vec{a}_m - \vec{b}_m), \quad \vec{c}_t = \vec{a}_m + 2\vec{c}_m. \quad (1)$$

The transformed lattice parameters obtained at 623 K are compared to the experimental values of phase I $CsHSO_4$ in Table VIII. There is a good agreement between the computed and experimental values. The cell angles are all 90° for both theory and experiment, whereas the simulation values of a =5.77 Å and c=14.66 Å compare well to the experimental values of 5.74 and 14.31 Å, respectively. Moreover, the positions of the Cs and S atoms (in the transformed, tetragonal coordinate system) are extremely close (0.001 for Cs and 0.0015 for S) to the measured values for the tetragonal phase, Table IX. Thus, the transition that occurs between 573 and 623 K, Fig. 6, correctly reflects the monoclinic phase II to tetragonal phase I transformation of $CsHSO_4$. A second transition is evident in the data at 698 K. For reasons provided below, we ascribe this to the melting of $CsHSO_4$.

The average internal structure of the HSO_4 groups remains essentially unchanged in the simulations as a function of temperature from that of the simulations at 298 K, Table VIII. This suggests that the superprotonic phase transitions can be predicted *without* precisely reproducing the specifics of the tetrahedral groups below and above the transition. It is also consistent with the observation that the absorption bands in the IR spectra of $CsHSO_4$ associated with the SO_4 group

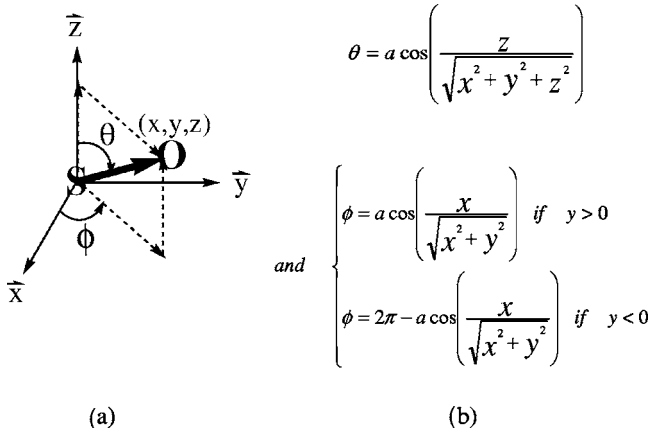

FIG. 9. Laboratory (fixed) frame and equations used to calculate the orientation of a tetrahedron's S-O_D vector.

internal modes are not affected by the transition.[18–20]

2. X-ray powder diffraction patterns

Further characterization of the structural evolution of $CsHSO_4$ as a function of temperature was carried out by examining the x-ray powder diffraction patterns at selected temperatures. To do so, the diffraction intensities (using CERIUS2[22]) for the instantaneous structure at each 0.1 ps of the final 150 ps were calculated and these 1500 patterns then averaged to obtain the time-averaged (XRDP) at each temperature. Results are presented for 298, 573 K (phase II), 623 K (phase I) and 723 K and compared to patterns simulated from the reported experimental atomic coordinates and lattice parameters, Fig. 7. It is clear that the patterns below 598 K are characteristic of phase II, Figs 7(b) and 7(c), whereas the pattern obtained at 623 K is characteristic of phase I, Fig. 7(e). The diffraction pattern obtained from the simulations at 723 K, Fig. 7(f), shows significantly less structure than the others, indicative of a liquid phase.

3. Volume and energy change across T_{sp}

The average potential energy and volume of the unit cell are shown as a function of temperature in Fig. 8. Jumps in the values of both of these quantities are apparent at 598 and 698 K. The first discontinuity is clearly a result of the transition of $CHSO_4$ to its superprotonic phase, whereas the large volume and enthalpy changes of the second discontinuity are consistent with melting. From a linear fit of the data in the phases II and I regions, the volume and enthalpy changes across the transition were quantified. The results, Table X, match the experimentally determined values very well. The simulated volume and enthalpy changes at 589 K are 1.6 kcal/mol and 1.7%, respectively, whereas the experimental values are 1.43 kcal/mol and 1.4%, respectively, for the superprotonic transition at 414 K. At the melting transition at 698 K the changes observed in the simulations are 2.1 kcal/mol and 5.7%, respectively.

Overall, it is apparent that the simulations are able to correctly predict the monoclinic to tetragonal phase transition of $CsHSO_4$ as well as the overall crystal chemistry of

TABLE X. Thermodynamics properties for the superprotonic phase transition in $CsHSO_4$.

	T_{sp} (K)	$\Delta(\text{volume})_{sp}$ (%)	$\Delta(\text{enthalpy})_s$ (kcal/mol)	T_m (K)	Stability range-$(T_m - T_{sp})$(K)
MD results	598	1.7	1.6	673	75
Experiment	414(1)	1.4(4)[a,b]	1.43(12)	485(2)	71(3)
Reference	2 and 37	11 and 38	37 and 39	40 and 41	2, 37, 40, and 41

[a]No direct measurement of transition volume change, extrapolated from structures and thermal expansion coefficients.

[b]Calculated from structural data. Note that the thermal expansion coefficient for phase II $CsHSO_4$ given in the paper Ref. 38 is inconsistent when compared to the printed data: listed as 0.056 cm^3/deg, but a direct calculation gives 0.035 cm^3/deg.

the compound within each of these phases. However, the transition temperature from the simulations is 184 K higher than experiment. The simplest explanation for this discrepancy is the need for longer equilibration times and, indeed, both the superprotonic and melting transitions occurred 25 K earlier when each simulation was run for 600 ps. The discrepancy is also likely due to the lack of proton transfer and the manner in which oxygen atoms have been classified into donor, acceptor, and nonhydrogen-bonded species in the present description. These are features of the low temperature but not the high temperature structure, and their inclusion in the model would be anticipated to favor the low temperature structure and delay the transition. Force field parameters affecting the phase transition temperature are investigated in more depth in the Appendix.

C. Phase transition: Dynamic properties

It should be noted that because the internal modes of the SO_4 group are largely unaffected by the transition, and this was observed in the simulations just as it has been documented experimentally, analysis of the IR spectra does not yield significant insight into SO_4 dynamics. Instead, we directly examine the positions of the oxygen atoms to reveal the SO_4 orientation and its evolution with time.

1. Orientations of the sulfate group

As noted above, a key feature of the experimentally observed structure of $CsHSO_4$-I is the presence of dynamically disordered SO_4 groups.[15] To provide a measure of the state of sulfate group disorder in the simulation, the orientation of a tetrahedron was defined in terms of the vectors between the central S atom and the four oxygen atoms. The coordinates defining the four S-O vectors for a particular sulfate group located within the central region of the simulation cell were recorded every 0.1 ps from 150 to 300 ps at each temperature step. [Selection of a centrally located tetrahedron eliminates the need to consider the effects of adjacent supercells on the calculated angles.] The orientation of these vectors relative

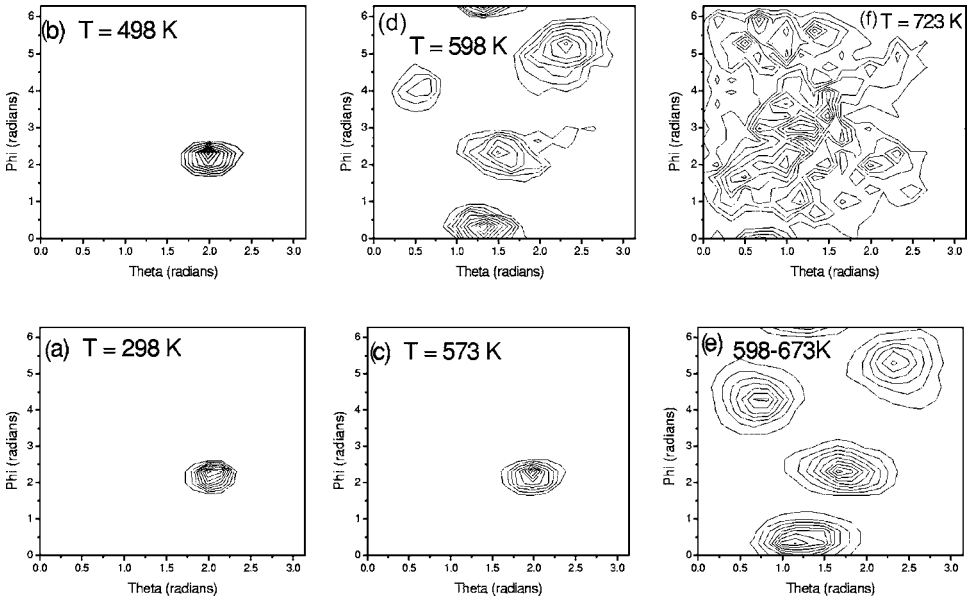

FIG. 10. Probability distribution functions for the S-O vectors: (a), (b), (c), (d), and (f) were created using only the orientations of the S85-O86 (donor oxygen) at 298, 498, 573, 598, and 723 K, respectively, whereas (e) is a combination of the orientations for *all four* S-O vectors of the S85 tetrahedron in the temperature range 598–673 K (phase I). The directions of the S-O vectors were converted into the polar coordinates (θ, ϕ) and then mapped onto the 2 D (θ, ϕ) space. A probability distribution function was created by partitioning the full ranges of each variable $(0 \leq \theta < \pi, 0 \leq \phi < 2\pi)$ into a 20×20 matrix and assigning each (θ, ϕ) pair to a particular cell.

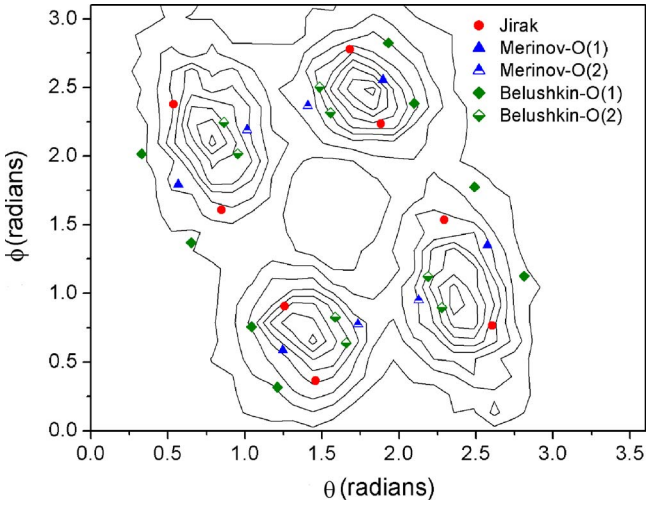

FIG. 11. (Color online) Probability distribution functions for all S-O vectors in phase I (from the 598–673 K simulations). The four distinct directions correspond fairly well to S-O directions derived from the published structures (Refs. 11, 13, and 14).

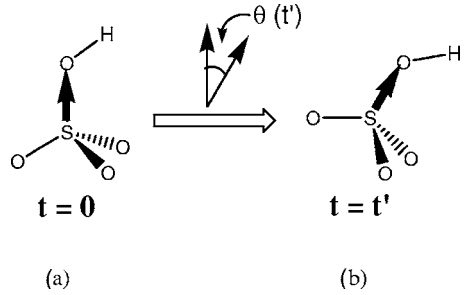

FIG. 12. Orientation/reorientation of HSO_4^- ion defined by its S-O_D vector: (a) an HSO_4^- ion has the vector pointing from its S to O_D atom initially aligned vertically; (b) after a time t', the HSO_4^- ion has changed its orientation and the S to O_D vector now forms an angle $\theta(t')$ with the vertical.

to a fixed (laboratory) reference frame, Fig. 9(a), were mapped onto a polar coordinate system with a particular direction (x,y,z) determining a pair of angels (θ,ϕ) using the standard equations shown, Fig. 9(b).

The orientations of selected S-O vectors (as defined in the polar coordinate system) at several temperatures are shown in the form of density maps in Figs 10 and 11. In these maps, each contour line represents a tenth of the maximum density of the plot. It is immediately clear that the S-O_D vector of $CsHSO_4$ phase II, Figs 10(a)–10(c) (298–573 K), takes on only one orientation, and thus that the SO_4 group remains essentially static. Immediately above the transition (598 K), however, this vector takes on four possible directions, Fig. 10(d). These directions coincide with the directions taken on by all four S-O vectors of this particular sulfate anion, over the temperature range 598–673 K, Fig. 10(e). The results indicate that the SO_4 group undergoes reorientations in such a manner that oxygen atoms (including the donor oxygen atom) exchange positions, in agreement with experimental observations.[14] Above the second transition at 698 K, the S -O_D vector takes on random orientations, Fig. 10(f), consistent with the interpretation of this phase as a liquid.

The S-O orientation data were then used to try and identify the likely high temperature structure. As described above, several models for the structure of $CsHSO_4$-I have been proposed, which differ in terms of the precise locations of the oxygen (and hydrogen) atoms. An orientation density map was generated using all 32×4 S-O vectors in the supercell and all the data for simulations in the 598 to 673 temperature range (over which phase I was observed). Application of the symmetry operators of space group $I4_1/amd$ (the space group symmetry of $CsHSO_4$-I) collapses the many different directions of the S-O vectors into the four orientations of a single representative SO_4 group with vectors located within the space $0\leqslant\theta<\pi, 0\leqslant\phi<\pi$, as shown in Fig. 11. These are essentially the same orientations as obtained from analysis of a single sulfate anion, Fig. 10(e), but with better counting statistics. Applying the symmetry operations present about the sulfur atom, which resides at Wycoff position 4a or 4b, would further collapse the four peaks in the orientation density map into one, but the resulting image (not shown) does not readily lend itself to interpretation. Superimposed on the density map obtained from the simulations are the S-O orientations implied by the three main structural models reported for $CsHSO_4$-I. The structure reported by Jirak *et al.* contains only one crystallographically distinct oxygen atom, whereas those of Beluskin *et al.* and Merinov *et al.* each contain two, as shown in Fig. 2.

There are substantial differences between the S-O orientations obtained from the simulations of $CsHSO_4$-I and the experimental models. In particular, the four density peaks from the simulation all exhibit single maxima, implying that, although the SO_4 group can exist in one of four orientations if the oxygen atoms are individually labeled, in the absence of such labeling, each of these orientations is identical. In contrast, the experimental data show either two or four oxygen positions exist within each of the four regions of high orientation density. This feature gives rise to multiple (either two of four) orientations for the sulfate group. It is apparent that while the simulations are in general agreement with experiment in terms of the broad regions of high orientation density, there is insufficient resolution within the data to reveal any kind of structure within the orientation density peaks and directly favor one or the other of the experimental models. Broad orientation density peaks in the real structure of $CsHSO_4$-I may, in fact, be responsible for the difficulty encountered in experimentally resolving the exact locations of the oxygen atoms. Overall, the sulfate group within $CsHSO_4$-I likely librates between local energy minima within each of these broadly defined orientation density peaks, and less frequently undergoes reorientation with the S-O vectors changing positions from orientation density peak to another. The rate of these reorientations is discussed in greater detail below.

An alternative means of measuring the difference between the computational and experimental models of the structure of $CsHSO_4$-I is to examine the width of the orientation density peak along the two angular directions θ and ϕ and compare that to the angular distances between the experimental positions within a single region of high orientation density.

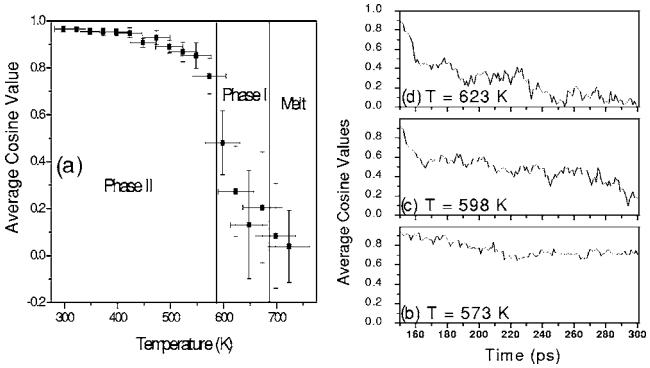

FIG. 13. Autocorrelation functions for all 32 tetrahedra evaluated using their average cosine values between the reference orientations (at 150 ps) and subsequent orientations: (a) average cosine value versus temperature. Note the decrease in the average cosine value across the phases II to I transition and that the average cosine values continue to decrease above the transition; (b) time dependence of the average cosine value at 573 K which equilibrates around 0.73, (c) same for 598, (d) same for 623 K, which drops to zero in 150 ps.

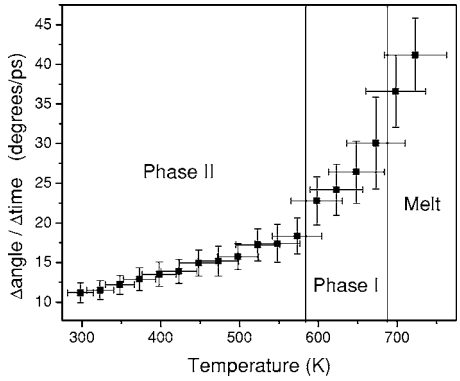

FIG. 14. Average angular velocity of all 32 $S-O_D$ vectors versus temperature. Note that the jump in this value at the phase II-I transition is only ~25%. Therefore the dramatic increase in protonic conductivity across the transition (100 000–1 000 000 %) is due to a change in the *nature* of the reorientations (e.g., oscillation to libration/rotation) rather than the *degree* of the reorientations.

Analysis of the computational results yields $\Delta\theta$ and $\Delta\phi$ values of 0.47(5) and 0.68(12) rad., Table XI, indicating larger librations along Φ than along θ. The experimentally determined structures of both Jirak *et al.*[11] and Belushkin *et al.*[14] similarly result in greater librational motion along ϕ than along θ, whereas the structure proposed by Merinov *et al.*[13] implies the opposite result. Thus, the simulations are in greater agreement with the Belushkin *et al.* and Jirak *et al.* structures than that of Merinov *et al.*.

2. *Types and rates of* HSO_4 *group reorientations*

The types and rates of HSO_4^- ions reorientations were next evaluated using a variety of measures: an orientation correlation function, the angular change of the orientation per picosecond, and the frequency of change from one orientation to the next. In all cases, the orientation of an HSO_4^- ion was defined by the vector pointing from its S to O_D atom, as was done above, Fig. 12.

The orientation correlation function implemented here, $F(t)$, was defined here in terms of the cosine of the angle θ_i between the orientation of the S-O_D vector $\vec{r}_i$ of any of the 32 sulfate tetrahedra in the computational cell, at the initial time t_o and its orientation at a later time. Specifically,

$$F(t) = \langle \cos(\theta_i) \rangle = \left\langle \frac{\vec{r}_i(t_o) \cdot \vec{r}_i(t)}{|\vec{r}_i(t_o) \cdot \vec{r}_i(t)|} \right\rangle,$$

where the average is taken over the $i=\{1,\ldots,32\}$ tetrahedra and the function is calculated in time steps of $\Delta t=1$ ps. In order to allow for equilibration effects, $t_o=150$ ps was taken for the initial state of the system. Much like a conventional autocorrelation function, $F(t)$, by definition, varies from 1 to 0, with a value of 1 indicating no change in the orientations of $\vec{r}_i$ relative to their original orientation and a value of 0 indicating a set of completely random orientations of $\vec{r}_i$. $F(t)$ was computed at three temperatures, one just below the phase II → I transition (573 K), one just above the transition (598 K), and one well within the existence range of phase I (623 K). In addition, the time averaged value of $F(t)$, $\overline{F(t)}$, was evaluated as a function of temperature, as was the standard deviation of this parameter.

The results of this analysis, Figs. 13(b)–13(d) show quite clearly that at temperatures below the transition ($T=573$ K), the sulfate group orientation remains relatively fixed, whereas just above the transition ($T=598$ K), the sulfate groups become almost completely randomly oriented after a period of 150 ps relative to their initial state. At higher temperatures ($T=623$ K), randomization occurs even more quickly, within about 100 ps, despite the persistence of phase

TABLE XI. Proposed librations in $CsHSO_4$ phase I compared to simulation results.

Source	Number of librations	Average $\Delta\theta$ (rad) between librations	Average $\Delta\phi$ (rad) between librations	$\Delta\phi-\Delta\theta$ (rad)	Reference
Merinov *et al.*	2	0.47	0.3	−0.17	13
Jirak *et al.*	2	0.3	0.66	0.36	11
Belushkin *et al.*	4	0.35	0.42	0.07	14
Simulation	N/A	0.47(5)	0.68(12)	0.21(17)	

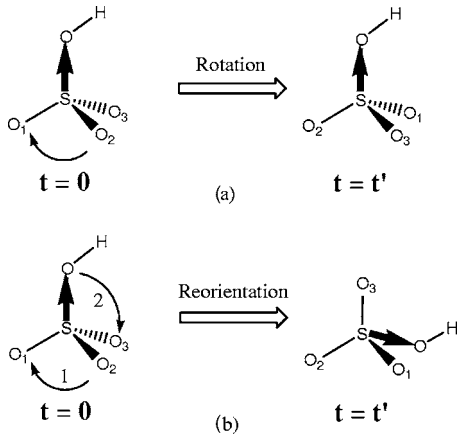

FIG. 15. Pictorial representation of the difference between a three-fold, axial rotation around the S-O_D vector and an extensive reorientation involving the S-O_D vector.

I under these conditions. The time averaged value of $F(t)$, Fig. 13(a), reveals that there is a sharp increase in the randomization of the sulfate group orientation (that occurs within 150 ps) upon passing through the phase II $\rightarrow$ I transition, with $F(t)$ dropping from 0.76 at 573 K to 0.48 at 598 K, followed by only a gradual increase in the extent of randomization as the material enters the molten state. This behavior is consistent with the description of near "free rotation" of the tetrahedra in phase I and in the melt.[20] Indeed, there is greater similarity between the molten phase and phase I than between phases I and II in terms of sulfate group reorientation dynamics.

The second method of quantification of the sulfate group reorientations, the average angular change per picosecond of the $S-O_D$ vector orientation, is simply given as

$$\Delta\theta(t_i)/\Delta t = [\theta(t_i - \Delta t) - \theta(t_i)]/\Delta t.$$

Again, for good statistics, the values for each of the 32 sulfate groups in the supercell were averaged, and the calculation performed as a function of temperature. The results, Fig. 14, show quite clearly that although there is a marked increase in the angular velocities of the sulfate groups upon passing through the phase II $\rightarrow$ I transition, it is not particularly dramatic ($\sim$25%). Thus, the speed with which the sulfate group moves from one orientation to the next cannot alone be responsible for the $\sim$4 orders of magnitude increase in the conductivity at the superprotonic transition.

Careful examination of the oxygen coordinates about a particular sulfate group in phase II (298–573 K) revealed that sulfate group reorientations occurred in one of two ways, Fig. 15. In the first, which we refer to as axial rotations, the O_D atom remained fixed while the remaining three ligands underwent a $\pi/3$ rad (60°) rotation (C_3 operation); in the second type of motion, which we refer to as extensive reorientations, all oxygen atoms exchanged positions and the new orientation is related to the original by two successive C_3 symmetry operations. The frequency of the axial rotations and extensive reorientations in phase II (298–573 K) was calculated by counting how many times three or all four oxygens, respectively, of a sulfate changed their orientation

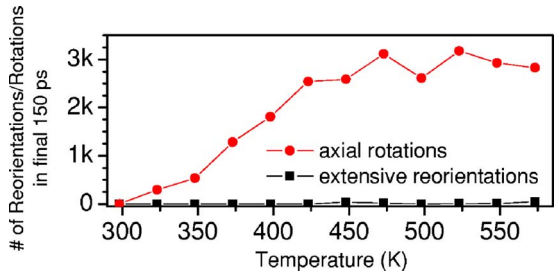

FIG. 16. (Color online) Rearrangements of the sulfate tetrahedra below the superprotonic phase transition at 598 K. Note the significant number of axial rotations (even near ambient temperatures), while the number of extensive reorientations remains at or very near zero.

by more than $\pi/2$ rad (i.e., 90°) over the last 150 ps of the simulation, in 1 ps steps. In principle it is possible for the sulfate group to undergo an axial rotation involving the O_D and two other oxygen atoms, however, few such rotations were observed and these were not subtracted from the number of axial rotations counted.

The results of the reorientation rate analysis are presented in Fig. 16. Consistent with the data presented in Figs. 10(a)–10(c), essentially no extensive reorientations occur prior to the transition. Quite unexpected is the high frequency of axial rotations that occur in the monoclinic phase prior to the superprotonic transition, being significant even at ambient temperatures. The commonly held view that the sulfate groups are static in this phase, derived primarily from diffraction analyses, may be an inappropriate simplification of the true behavior of $CsHSO_4$-II. A similar type of threefold rotation was proposed to explain the results of H^+ NMR studies on KH_2PO_4.[42,43] This behavior may well be a general phenomenon in solid acid proton conductors in their nonsuperprotonic phases, and the gradual rise in the frequency of the reorientations may explain the gradual increase in conductivity typically observed as a solid acid compound is heated to its superprotonic transition. For further discussion of force field parameters affecting these reorientation and rotation rates see Sec. II in the Appendix .

At temperatures above the transition (598–673 K), it was found that definitions employed for rotations and reorientations were no longer appropriate because the large amplitude of thermal vibrations precluded distinction of true changes in orientation of the sulfate group from simple librations. Instead, reorientations/rotations were evaluated in terms of the orientation of the S-O_D vector with respect to its probability distribution function, Figs. 10(e) and 11. Specifically, a reorientation was taken to occur if the S-O_D vector changed orientation from one region of high orientation density to another. In this case, no distinction between threefold axial rotations and extensive reorientations was made. The calculation was performed under two different definitions for the full width at half maximum (FWHM) values for the peaks in the probably density contour plots. In the first case, the average values, 0.47 rad in θ and 0.68 rad in ϕ, were employed, and in the second, these averages were increased by their respective standard deviations and the values of 0.52 rad in θ and 0.80 rad in ϕ were utilized.

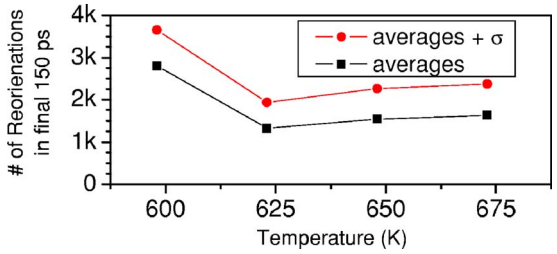

FIG. 17. (Color online) Sulfate group reorientations involving the donor oxygen for simulations exhibiting the superprotonic phase of $CsHSO_4$ (598–673 K). Numbers were calculated using two sets of FWHM values for the regions of high orientational density in Fig. 11: 0.47 rad in θ and 0.68 rad in ϕ (the average values) and 0.52 rad in θ and 0.80 rad in ϕ (the averages increased by their respective standard deviations).

Figure 17 shows the number of such reorientations as a function of temperature (over the last 150 ps of the simulation, in 0.1 ps steps). Above the transition, several thousand reorientations were observed at each temperature. In contrast, below the transition (data not shown in Fig. 17), no more than ten such reorientations occurred, as evidenced by the probability density plots of Figs. 10(a)–10(c). These reorientations are thus the key dynamic feature of the superprotonic transition. Within the temperature range of 598 to 673 K, there is an initial drop in the rate of reorientations (from 598 to 623 K), followed by a general increase (from 623 to 673 K). We attribute the initial drop to an artifact of the incomplete transition at 598 K. The presence of both the monoclinic and tetragonal phases in the supercell at 598 K [see Fig. 5(a)] may cause the material to effectively display greater disorder than even phase I $CsHSO_4$. The gradual increase in the number of reorientation from 623 to 673 K is expected for a thermally activated process. The activation energy derived from these data (in the range 623–673 K) is approximately 0.2 eV. To compare with experimental values for proton transport, we must add to this calculated *rotational* activation energy the measured value for proton hopping, 0.1 eV.[44] This is due to the fact that the Grotthuss mechanism for proton transport requires tetrahedral reorientations in conjunction with inter tetrahedral proton hopping,[1] but these simulations explicitly prohibited proton hopping. Adding the simulated rotational and measured hopping activation energies then gives a total activation energy for proton transport in the superprotonic phase of $CsHSO_4$ of 0.3 eV. This value is in excellent agreement with the experimentally measured activation energy of 0.27–0.30 eV.[3,17,45,46] In addition, the overall sulfate group reorientation rate (averaged over the temperature range 598–673 K) is $\sim 5 \times 10^{11}$/s which also agrees extremely well with the experimentally determined rate of $\sim 10^{12}$/s.[15]

V. SUMMARY AND CONCLUSIONS

The superprotonic phase transition (phase II → phase I; 414 K) of $CsHSO_4$ was simulated by classical molecular dynamics methods over the temperature range of 298 to 723 K. The Drieding force field formalism was employed,[21] but

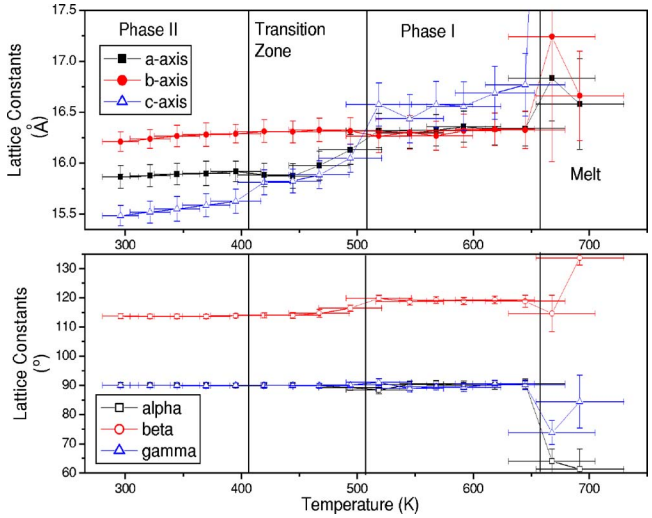

FIG. 18. (Color online) Unit cell parameters as a function of temperature, as obtained from MD simulations using equal charges on all four oxygens. The superprotonic transition initiates at 423 K and is complete (i.e., $\beta = 120°$ and $|a| = |b|$) at 523 K.

with the FF parameters appropriately adjusted so as to reproduce structural and energetic quantities derived from quantum mechanical calculations performed on small clusters involving the elements of $CsHSO_4$. Specifically, the S, O, and H parameters were adjusted to reproduce the QM-derived structure and frequencies of a gas-phase $CsHSO_4$ monomer. Cesium vdW parameters were modified to duplicate the QM binding energy, average Cs-O distance, and symmetric-stretch frequency of the monomer. Hydrogen bond parameters were adjusted to reproduce the QM O_D-O_A distance and binding energy of a gas-phase $(H_2SO_4)_2$ dimer. The hydrogen torsional barrier height of the HSO_4^- groups was fit to a series of QM calculations on HSO_4^- ion including Poison Boltzmann solvation.

The simulations reproduce, to a high level of accuracy, several structural and dynamic features of $CsHSO_4$ in both its monoclinic phase (phase II) and superprotonic, tetragonal phase (phase I). Furthermore, the transition itself is predicted, without any experimental input that would require *a priori* knowledge of the existence of a superprotonic phase. Thus, in principle, this approach is applicable to compounds for which experimental data are not available, and even to hypothesized compounds should a reasonable starting point of the room temperature structure be available. The systematic and straight-forward method by which the FF parameters were adjusted from the Drieding defaults to values specific to $CsHSO_4$ was also developed with the goal of establishing a protocol for probing the behavior of the broad range of compounds containing oxyanion groups linked by hydrogen bonds. For example, one may be able to utilize such MD studies to explain why a compound such as $RbHSO_4$[37] (apparently) does not have a superprotonic transition under ambient pressure, and also to establish whether a compound such as $LaHSiO_4$, which is as yet unreported but certainly plausible, will exhibit superprotonic behavior.

In these simulations, the hydrogen was treated as bonded exclusively to a single oxygen atom (proton donor), with

TABLE XII. Changes in phase transition values due to adjusted FF parameters.

Simulation run	$T_{\text{low temp. trans.}}^{-}$ onset (K)	T_{sp}^{-} onset (K)	T_{sp}^{-} final (K)	T_m onset (K)	Stability range-$(T_m - T_{sp})$ (K)
Original	N/A	598	598	673	75
Equal oxygen charge	N/A	423	523	673	150
H-bond strength $\times 1.5$	348	623	623	673	50
H-bond strength $\times 2.0$	378	623	N/A	673	N/A
Torsional barrier $\div 10$	348	473	523	673	150
Torsional barrier $\times 10$	N/A	523?	648	698	50

hydrogen bonds extending to other nearby oxygen atoms (proton acceptors). Moreover, oxygen atoms were assigned (fixed) charges more appropriate for the structurally ordered phase II than the disordered phase I. Proton diffusion (i.e., proton jumps) between oxygen atoms cannot occur in this formalism. Nevertheless, the simulations showed a clear phase transition at 598 K. The discrepancy from the experimental transition temperature of 414 K is attributed to the rigid manner in which oxygen charges and hydrogen bonds are treated in the Dreiding FF (and is discussed further in the Appendix). Evidence of the phase transition was present in the change of lattice parameters, x-ray powder diffraction patterns, enthalpy, and volume of the cell as well as the direction and degree of reorientation of the HSO_4 groups. The amplitude of the fluctuations in the orientations of the HSO_4 groups rises dramatically above the transition temperature suggesting that the sharp increase of the proton conductivity arises from the nearly free rotation of the tetrahedra, as proposed previously in the literature.[7,47] These simulation results show that proton diffusion is *not* essential to the existence of a superprotonic phase transition, and that rotational disorder of HSO_4 groups is a sufficient condition to predict the presence of such transitions.

In sum, these simulations, in which a "first principles" *MSXX* FF derived only from the generic Dreiding FF and QM calculations is employed, have reproduced both the structural and dynamic properties of the superprotonic phase transition of $CsHSO_4$. A general approach was utilized to determine the FF parameters from QM that can be applied to other systems. Ultimately, this might enable rapid computational screening using theory to "discover" new superprotonic conducting compounds.

ACKNOWLEDGMENTS

We thank Lang Yang for her help with the probability distribution functions in Figs. 10 and 11. Financial support was provided by the National Science Foundation and acknowledgment is made to the Donors of the American Chemical Society Petroleum Research Fund, for partial support of this research.

APPENDIX: PARAMETERS AFFECTING THE PHASE TRANSITION TEMPERATURE

As described above, the MD simulations reported here reproduce quite well the structural and dynamic characteristics of $CsHSO_4$ in its room and high temperature phases, while also predicting the transition itself. However, as also noted above, agreement between the simulations and experiment with respect to the temperature of the transition is poor: 598 K from the simulations versus 414 K from experiment. This suggests that although the force field parameters correctly describe the interatomic interactions within $CsHSO_4$ in both phases II and I, some particular aspect of the force field retards the transition. Here we explore which force field parameters may be responsible for this effect.

It must be noted at the outset that the use of a FF formalism that restricts proton hopping (by uniquely defining the donor oxygen atoms in the structure) certainly favors phase II over phase I and is surely, in part, responsbile for the difference between the simulated and experimental phase transition temperatures. In addition, superheating, which occurs because of the short time scales of the simulations relative to the experimental time scales, may also play a role. Indeed, doubling the simulation time for each time step (without making any other changes) lowered the transition temperature by 25 K (one temperature interval). While these two effects—immobility of protons and superheating—are important (and motivate efforts to develop reactive force fields and more efficient computation methods), even within the framework of the FF used here, several parameters have major impact on the transition.

A priori, one expects that parameters delaying the onset of the superprotonic transition would be those that inhibit the "free" reorientation of the sulphate groups. Thus, this Appendix focuses on the parameters that govern the coupling of HSO_4^- to HSO_4^- and HSO_4^- to Cs^+ interactions, in particular, the distribution of charge on the oxygen atoms, the hydrogen bond strength, and the hydrogen torsional barrier height. The effect of these three quantities on the transition temperture was evaluated by performing the MD simulations after changing one (and only one) of these three parameters, with all other FF parameters identical to that found in Table II. The details of how these changes were implemented are provided below. The results of these simulations are summarized in Table XII. It is immediately evident that, while the phase II $\rightarrow$ I transition is impacted, none of these parameters has much effect on the onset of melting. This suggests that the total electrostatic energy, which changes little between the simulations, governs the melt temperature, as might be expected for an ionic solid. In what follows we provide an interpretation for the changes that occur to the superprotonic

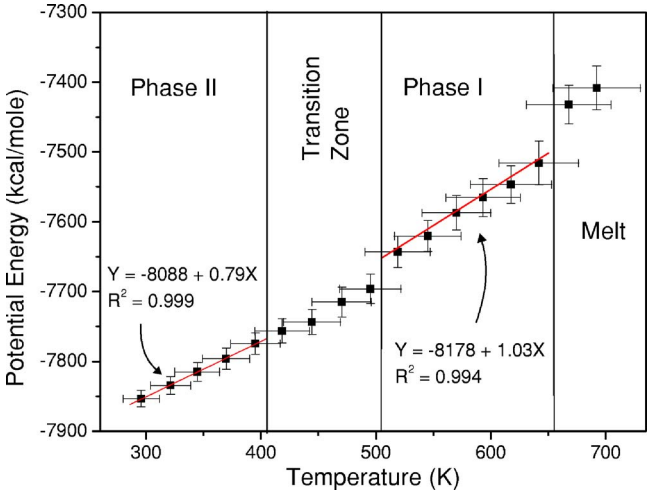

FIG. 19. (Color online) Potential energy as a function of temperature, as obtained from MD simulations using equal charges on all four oxygens. Discontinuities in the potential energy function are apparent at 523 K, at the completion of the superprotonic transition, and at 673 K, at the melting transition.

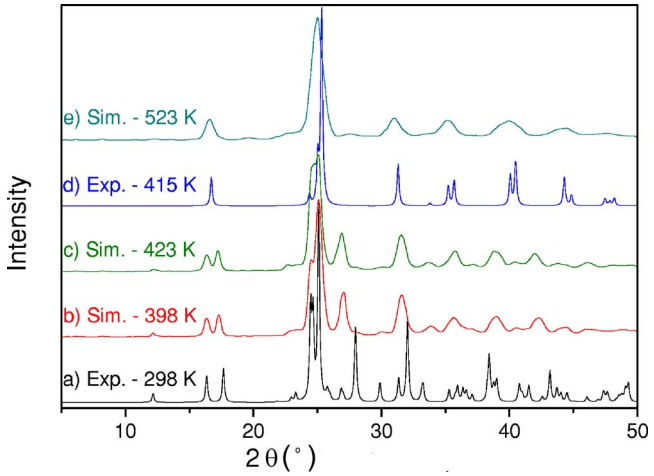

FIG. 20. (Color online) Calculated x-ray diffraction patterns: (b), (c), and (e) from MD simulations using equal oxygen charges at the temperatures indicated, (a) from the structure determined by single crystal x-ray diffraction at 298 K (Ref. 11) and (d) from structure determined by powder x-ray diffraction at 415 K (Ref. 10). Comparison of the patterns in (a), (b), and (c) show that the simulations at 398 and 423 K are in phase II $CsHSO_4$, whereas the diffraction pattern at 523 K, (e) matches the phase I pattern calculated from experiment (d).

transition temeprature for each modification to the force field parameters. Furthermore, we present evidence for an additional lower temperature transition, noted in Table XII, that seems to occur in some of the simulations

Oxygen charge distribution

As described in the main text, the ESP (electrostatic-potential-fitted) charges of the oxygen atoms were established from quantum mechanical calculations performed on the gas phase $CsHSO_4$ monomer. The QM values were slightly modified in the MD simulations such that the two oxygen atoms not participating in hydrogen bond formation had equal charges to one another, being greater than the charge of the acceptor oxygen atom, in turn greater than the charge of the donor oxygen atom. In superprotonic $CsHSO_4$ the time averaged charge for all of the oxygen atoms is the same because each participates equally in hydrogen bond formation (again, when averaged over time). To mimic this situation, we thus assigned a charge of $-0.612|e|$, equal to the average of the four charges in Table III. The results of these simulations, cell parameters as functions of temperature, potential energy as a function of temperature, and selected diffraction patterns, are presented in Figs. 18–20, respectively. In Fig. 20 the diffraction patterns obtained from the MD simulations are compared to the patterns of $CsHSO_4$ in phases I and II, simulated on the basis of experimental data.[10,11]

Assigning the oxygen atoms equal charges has a dramatic impact on the transition temperature, Figs. 18–20. The onset of the superprotonic transition occurs at 423 K, substantially lower than in any of the other simulations, Table XII. In general terms, this result reflects the dominance of electrostatics on the the binding energy of ionic solids.[48] For the $CsHSO_4$ in particular, the homogeneous distribution of charge favors the superprotonic phase, in which all oxygen atoms are identical over time and therefore carry equal *average* charge.

In addition to a reduction in the onset temperaturature of the superprotonic transition, modification of the oxygen charges has the effect of broadening the transition regime (such that it occurs over a 100 K range and $|c|>|a|=|b|$ at 523 K), and of inducing structural changes even before the transition itself. In particular, there is a signficant increase in the *c*-axis lattice constant from 398 to 423 K, Fig. 18. Detailed analysis showed this to correspond to a straightening of the zig zag $[HSO_4^-]_\infty$ chains in the structure (without any phase transition). These changes again emphasize the importance of electrostatics on the behavior of $CsHSO_4$.

The results demonstrate that the superprotonic transition is highly sensitive to the distribution of charge on the anions. Equal charges reduces the onset temperature of the transition by 175 deg (with respect to the original simulations), to a value just above the experimental transition temperature of 414 K. From our QM calculations (main text) it is clear that the oxygen atoms do not carry equal charge in the low temperature phase, but they presumably do, at least on average, at high temperature. Thus, a MD approach that allows the oxygen atoms to dynamically adjust their charge in response to the local environment would be most appropriate for an accurate prediction of superprotonic behavior. Implementation of a reactive force field approach to address this challenge, and simultaneously allow for proton migration, is underway and will be the subject of future reports.

Hydrogen bond strength

To evaluate the effect of hydrogen bond strength parameter on the superprotonic transition, we must define the

strength of a hydrogen bond used in these simulations. The strength of a hydrogen bond usually refers to the energy required to dissociate the $O_D-H\cdots O_A$ complex which, in turn, is highly correlated to the O_D-O_A distance: The smaller the donor to acceptor distance, the greater this dissociation energy and vice versa.[49,50] Hence, one way to increase/decrease the hydrogen bond strength is to shorten/lengthen the equilibrium O_D-O_A distances in the simulations, in particular, by modifying the parameter R_O (Table III) describing hydrogen bond interactions. However, it is not possible to modify hydrogen bond lengths in isolation, i.e., without changing other features in the overall structure which might themselves have significant impact on the transition. Consequently, instead of using hydrogen bond length as a proxy measure of hydrogen bond strength we maintained a fixed hydrogen bond length and defined the bond strength in terms of the binding energy of the H_2SO_4 dimer. Specifically, the hydrogen bond parameters (R_O and D_O) were simultaneously adjusted to modify the binding energy of the force field energy minimized $(H_2SO_4)_2$ molecule, *while maintaining* a fixed equilibrium O_D—O_A distance of 2.647 Å. Unfortunately, by this procedure it is not possible to appreciably ***de***crease the hydrogen bond strength, because of a compensating increase in electrostatic energy. However, it is possible to ***in***crease the hydrogen bond strength, and thus simulations were performed using hydrogen bonds that were 1.5× and 2× the strength of the original hydrogen bonds. Analysis of the simulations carried out at 298 K confirmed that the desired hydrogen bond length was maintained in the crystalline structure of $CsHSO_4$.

While the impact of changes to the hydrogen bond strength are not as dramatic as those of changes to the oxygen atom charges, we clearly observe that increasing the hydrogen bond strength favors the ordered structure of phase II over that of ordered phase I, raising the onset temperature of the transition by 25 K for both simulations, Table XII Morever, in the case of the simulations with twice the original hydrogen bond strength, phase I was sufficiently destabilized such that the phase II → I transformation was not complete before the onset of melting. Accompanying the energetic stablization of the ordered phase II is a dramatic reduction in the frequency of sulphate group axial rotations (see main text for precise definition) that occur in this phase, Fig. 21. Doubling the hydrogen bond strength reduces the frequency by as much as an order of magnitude at 398 K. These results suggest that the pre transition rotational disorder drives the transition, and, by retarding these, the transition itself is retarded. The results further indicate that, while it is not entirely clear how one can experimentally create a compound with weaker hydrogen bonds, such a material may exhibit structural disorder and superprotonic conductivity at reduced temperatures and thus over a wide temperature regime.

Careful examination of the unit cell dimensions (data not shown), reveal a subtle transition in $CsHSO_4$ at precisely the temperature at which the sulfate group axial rotation rate rises to a clearly non zero value. The basic structural features, as revealed by the diffraction patterns, are those of phase II both above and below this transition, with the two forms being distinguished by the frequency of axial rotations. For the doubled hydrogen bond strength simulations,

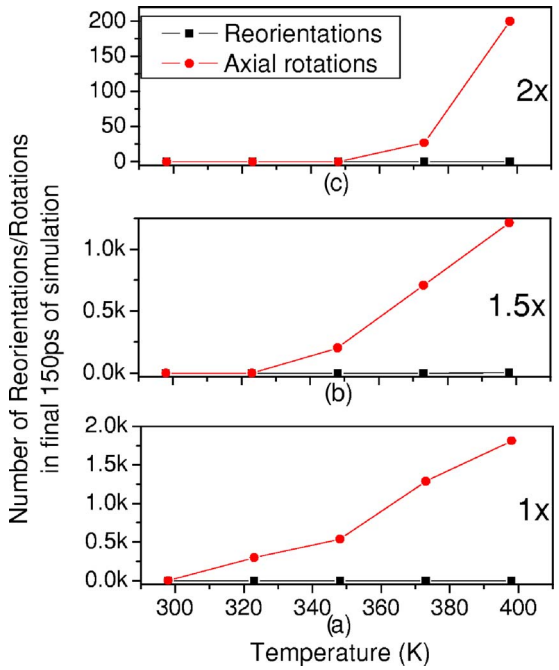

FIG. 21. (Color online) Rearrangements of the sulfate tetrahedra across the low temperature transitions of the simulations with increased hydrogen bond strength: (a) 1, (b) 1.5, and (c) 2 times the original hydrogen bond energies. Note the jump in axial rotations at precisely the same temperatures the lattice constants were observed to change, (Ref. 51), while the number of (extensive) reorientations remains at or very near zero.

the transition occurs at 378 K, whereas for the 1.5× simulations, it occurs at 348 K. The accompanying volume changes are −1.0 and −0.7 %, respectively (on heating). The changes in potential energy at the transition are below the error bounds of the simulations. In the case of the original force field, significant sulfate group rotations occur at all temperatures examined and thus any analogous transition must occur below 289 K.

The features of this low temperature transition are reminiscient of the phase III → II transition in $CsHSO_4$, although it must be emphasized that increasing the hydrogen bond strength did not induce $CsHSO_4$ to crystallize in the phase III structure in our simulations. Experimental measurements show that there is a decrease in volume of ~1% at the phase III → II transition[38] (comparable to that observed in the simulations), and the enthalpy change is only ~0.12–0.24 kcal/mol.[40] This equates to ~1–2 kcal/mol for the supercell and would be outside of the resolution limits of the simulations. The (experimental) hydrogen bond length in phase III is 2.54(1),[38] as compared to 2.636(5) in phase II,[38] implying hydrogen bond strengths[50] of 11 and 7.5 kcal/mol, respectively. The greater strength of the hydrogen bond of phase III is comparable to the higher hydrogen bond strengths introduced into these modified simulations (albeit at fixed hydrogen bond length). Finally, Raman and infrared spectroscopy studies indicate a substantial increase in sulfate group rearrangements across the phase III → II transition.[20] Such behavior is consistent with the changes observed at the transition in the simulations if one considers only the axial

rotations and not the extensive reorientations. The occurrence of these axial rotations may resolve the discrepancy between the spectroscopic studies, which point to dynamic sulfate groups, and the diffraction studies, which point to static sulfate groups in $CsHSO_4$-II (Ref. 38) without the need to invoke the notion of cyclic dimers.[10]

Torsional barrier height

To test the assumption that a lowered/increased torsional barrier would decrease/increase the superprotonic transition temperature, the value of the hydrogen torsion barrier was divided/multiplied by ten, from 2.1699 to 0.21699/21.699 kcal/mole, and the simulations rerun with no other changes to the original FF. Using the lowered torsional barrier, the simulations obtain a decreased phase II to I transition , beginning at 473 K and finishing at 523 K, 75 deg lower than the original simulations, Table XII. These simulations also show a low temperature transition at 348 K similar to those seen in simulations using an increased hydrogen bond strength. However the simulation with increased torsional height leads to more complicated results, with the transition starting at 523 K and finishing at 648 K, Table XII. Therefore the onset temperature is 75 K lower, while the final arrival at phase I is 50 K higher than the 598 K value of the original simulations.

These two effects would appear to be contradictory. *A priori*, one would expect that an increase in the torsional barrier would raise the thermal energy required for the transition to phase I, and thereby to increase in the transition temperature. The lower onset temperature found in the simulations suggests that the high torsional barrier energetically favors phase I over phase II. This dilemma is most simply explained by the destabilization of phase II due to a conflict between the increased tetrahedral reorientations and the rigidity imposed on the hydrogen by the high torsional barrier. An autocorrelation function (see Sec. IV C 2) for these simulations, Fig. 22, shows a small but significant amount of tetrahedral reorientations in phase II. The hydrogen bonds in phase II will become more and more distorted as these reorientations increase because of the reduced ability of hydrogen atoms to cross the torsional barrier. Hence, the lower onset temperature possibly results from a compromise between the energy required to rearrange the pertinent atoms and the hydrogen bond energy regained in the process. The higher arrival temperature in phase I then supports the assertion that increased torsional barrier heights hinder the phase II–I transition.

A comparison of the two autocorrelation functions for the lower and higher torsional barrier simulations reveals that the average cosine values of the lower/higher barrier runs is consistently smaller/bigger than those of the original MD simulations [Fig. 13(a)] at all temperatures. This systematic difference equates to a greater/lesser degree of tetrahedral reorientations for the lower/higher barrier simulations, as expected. The change of the average cosine values with temperatures above the onset transition is also quite different for the two simulations, with a rapid fall for the low barrier runs, versus a gradual decrease for the high barrier. This result

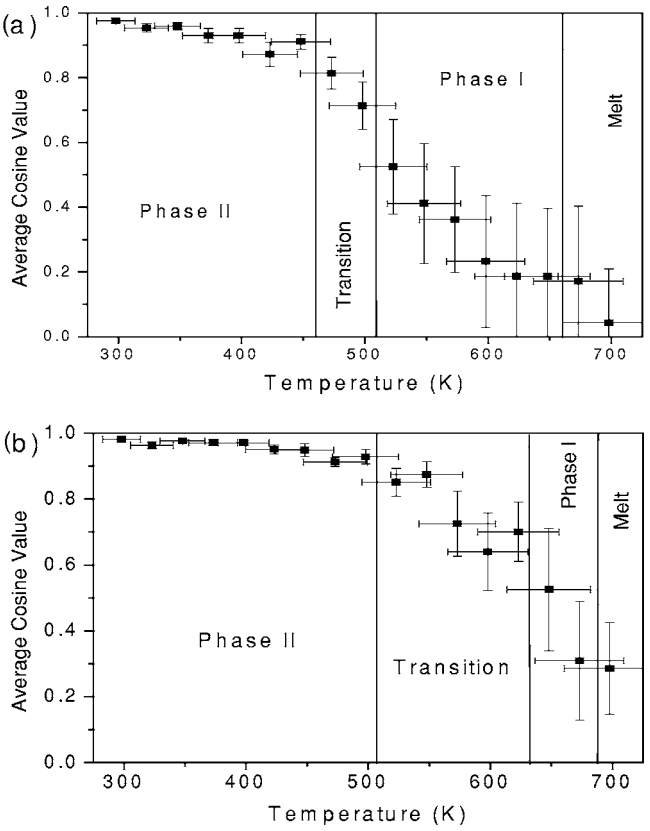

FIG. 22. Autocorrelation functions for simulations with (a) decreased and (b) increased torsional barrier heights. The values are lower in (a) and higher in (b) when compared to the original simulations Fig. 13(a).

agrees with the previous arguments as the low and high torsional barriers should increase/decrease the rotational ability of the sulfate groups generated by the structural changes. The results of these simulations are discussed in more detail elsewhere.[51]

Conclusions

The importance of the oxygen charge distribution hydrogen, hydrogen bond strength, and torsional barrier height to the transition temperature was probed; the relevant parameter was changed independently of the other two and the series of simulations repeated. The results are in agreement with *a priori* arguments that any changes to the force field parameters inhibiting the rotations of the HSO_4 groups will increase the temperature of the transition, whereas changes enhancing rotations lower the transition temperature. Of particular interest are the results of the simulations in which all oxygen electrostatic charges were set to equal values. These simulations lead to an onset of the transition at 423 K, just above the experimental value of 414 K.[2] This drop provides further evidence that rotational reorientation dominates the phase transition. These results emphasize the importance of using a FF in which the charges continuously readjust for the local environment and allow for proton migration between the tetrahedral.

*Corresponding author. Electronic address: wag@wag.caltech.edu

[1] K. D. Kreuer, Th. Dippel, N. G. Hainovshy, and J. Maier, Ber. Bunsenges. Phys. Chem. **96** 1736 (1992).
[2] M. Komukae, T. Osaka, Y. Makita, K. Itoh, and E. Nakamura, J. Phys. Soc. Jpn. **50**, 3187 (1981).
[3] A. I. Baranov, L. A. Shuvalov, and N. M. Shchagina, JETP Lett. **36**, 459 (1982).
[4] S. Chandra, *Proton Conductors* (Academic, San Diego, 1989).
[5] K.-D. Kreuer, Chem. Mater. **8**, 610 (1996).
[6] W. Munch, K. D. Kreuer, U. Traub, and J. Maier, Solid State Ionics **77**, 10 (1995).
[7] W. Munch, K. D. Kreuer, U. Traub and J. Maier J. Math. Phys. **381**, 1 (1996).
[8] A. V. Belushkin, I. Natkaniec, N. M. Pakida, L. A. Shuvalov, and J. Wasicki, J. Phys. C **20**, 671 (1987).
[9] A. M. Balagurov, A. V. Belushkin, I. D. Dutt, I. Natkaniec, N. M. Plakida, B. N. Savenko, L. A. Shuvalov, and J. Wasicki, Ferroelectrics, **63**, 59 (1985).
[10] C. R. I. Chisholm, and S. M. Haile, Mater. Res. Bull. **35** 999 (2000).
[11] Z. Jirak, M. Dlouha, S. Vratislav, A. M. Balagurov, A. I. Beskrovnyi, V. I. Gordelii, I. D. Datt, and L. A. Shuvalov, Phys. Status Solidi A **100**, K117 (1987).
[12] P. Colomban, and J. C. Badot, J. Phys.: Condens. Matter **4** 5625 (1992).
[13] B. V. Merinov, A. I. Baranov, L. A. Shuvalov, and B. A. Maksimov, **32**, 86 (1987).
[14] A. V. Belushkin, W. I. F. David, R. M. Ibberson, and L. A. Shuvalov, Acta Crystallogr., Sect. B: Struct. Sci. **B47** , 161 (1991).
[15] J. C. Badot, and Ph. Colomban, Solid State Ionics **35**, 143 (1989).
[16] A. I. Baranov, Izv. Akad. Nauk SSSR, Ser. Fiz. **51** 2146 (1987).
[17] R. Blinc, J. Dolinsek, G. Lahajnar, I. Zupancic, L. A. Shuvalov, and A. I. Baranov, Phys. Status Solidi B **123**, 83 (1984).
[18] J. Baran, and M. K. Marchewka, J. Mol. Struct. **614**, 133 (2002).
[19] V. P. Dmitriev, V. V. Loshkarev, L. M. Rabkin, L. A. Shuvalov, and Yu. I. Yuzyuk, Sov. Phys. Crystallogr. 1986, **31**(6), 673-677.
[20] M. Pham-Thi, Ph. Colomban, A. Novak, and R. Blinc, J. Raman Spectrosc. **18**, 185 (1987).
[21] S. L. Mayo, B. D. Olafson, and W. A. Goddard III, J. Phys. Chem. **94**, 8897 (1990).
[22] CERIUS2 4.0 Molecular Simulations Inc..
[23] Y. H. Jang, X. Y. Chang, M. Blanco, S. G. Hwang, Y. C. Tang, P. Shuler, and W. A. Goddard, J. Phys. Chem. B **106**, 9951 (2002).
[24] J. C. Slater, *Quantum Theory of Molecules and Solids., Vol 4., The Self-Consistent Field for Molecules and Solids* (McGraw-Hill, New York, 1974).
[25] A. D. Becke, Phys. Rev. A **38**, 3098 (1988).
[26] S. H. Vosko, L. Wilk, and M. Nusair, Can. J. Phys. **58**, 1200 (1980).
[27] C. T. Lee, W. T. Yang, and R. G. Parr, Phys. Rev. B **37**, 785 (1988).
[28] B. Miehlich, A. Savin, H. Stoll, and H. Preuss, Chem. Phys. Lett. **157**, 200 (1989).
[29] P. J. Hay and W. R. Wadt, J. Chem. Phys. **82**, 299 (1985).
[30] JAGUAR V.3.5 Schrodinger, Inc.
[31] D. J. Tannor, B. Marten, R. Murphy, R. A. Friesner, D. Sitkoff, A. Nicholls, M. Ringnalda, W. A. Goddard, and B. Honing, J. Am. Chem. Soc. **116**, 11875 (1994).
[32] L. E. Chirlian, and M. M. Francl, J. Comput. Chem. **8**, 894 (1990).
[33] S. Nose, Mol. Phys. **52**, 255 (1984).
[34] W. G. Hoover, Phys. Rev. A **31**, 1695 (1985).
[35] X. Ke, and I. Tanaka, Phys. Rev. B **69**, 165114-1 (2004).
[36] V. Varma, N. Rangavittal, and C. N. R. Rao, J. Solid State Chem. **106**, 164 (1993).
[37] M. Friesel, B. Baranowski, and A. Lundén, Solid State Ionics **35**, 85 (1989).
[38] J. Lipkowski, B. Baranowski, and A. Lunden, Pol. J. Chem. **67**, 1867 (1993).
[39] D. A. Boysen, C. R. I. Chisholm, S. M. Haile, and S. R. Narayanan, J. Electrochem. Soc. **147**, 3610 (2000).
[40] B. Baranowski, M. Friesel, and A. Lundén, Physica A **156**, 353 (1989).
[41] M. Pham-Thi, Ph. Colomban, A. Novak, and R. Blinc, Solid State Commun. **55**, 265 (1985).
[42] R. Blinc, J. Stepismilk, M. Jamsek-Vilfan, and S. Zumer, J. Chem. Phys. **51**, 187 (1971).
[43] R. Blinc, and J. Pirs, J. Chem. Phys. **54**, 1535 (1971).
[44] A. V. Belushkin, C. J. Carlile, and L. A. Shuvalov, J. Phys.: Condens. Matter **4**, 389 (1992).
[45] T. Norby, M. Friesel, and B. E. Mellender, Solid State Ionics **77**, 105 (1995).
[46] V. V. Sinitsyn, E. G. Ponyatovskii, A. I. Baranov, A. V. Tregubcheko, and L. A. Shuvalov, Sov. Phys. JETP **73**, 386 (1991).
[47] P. Zetterström, A. V. Belushkin, R. L. McGreevy, and L. A. Shuvalov, Solid State Ionics **116**, 321 (1999).
[48] L. Pauling, *The Nature of the Chemical Bond* (Cornell University Press, Ithica, New York, 1960).
[49] P. Schuster, G. Zundel, and C. Sandorfy, *The Hydrogen Bond* (North-Holland, P Amsterdam, 1976).
[50] E. R. Lippincott, and R. Schroeder, J. Chem. Phys. **23**, 1099 (1955).
[51] C. R. I. Chisholm, Ph. D. thesis, California Institute of Technology, Pasadena, CA.